Stochastic Structural Stability Theory for roll/streak formation in forced and free wall bounded shear flow turbulence

BRIAN F. FARRELL[1] AND PETROS J. IOANNOU[2]

[1]Department of Earth and Planetary Sciences, Harvard University, Cambridge, MA 02138, USA

[2]Department of Physics, University of Athens, Panepistimiopolis, Zografos, 15784, Greece

(Received 14 May 2011)

Stochastic Structural Stability Theory (SSST) employs an ensemble mean stochastic turbulence model (STM) for perturbation dynamics coupled to the streamwise mean flow dynamics to obtain an autonomous, deterministic, nonlinear dynamical system for evolving an approximate statistical mean turbulent state. In this work SSST is applied to the problem of understanding growth, maintenance, and breakdown of the roll/streak structures that occur in association with forced and free turbulence in neutrally stratified wall bounded shear flow. Roll structures in the cross-stream/spanwise plane and associated streamwise streaks are shown using this analysis to grow through an emergent coherent eddy/mean-flow interaction. In this interaction incoherent Reynolds stresses arising from mechanically forced turbulence are organized by perturbation streamwise streaks to coherently force perturbation rolls giving rise to an amplification of the streamwise streak perturbation and through this feedback to exponential growth of the combined roll/streak/turbulence complex. The dominant turbulent eddy structures involved in producing the roll/streak/turbulence complex instability are non-modal perturbations with the form of oblique waves. Over a range of parameters this instability equilibrates nonlinearly to form finite amplitude roll/streak coherent structures. However, for sufficiently high levels of forced turbulence the roll/streak complex becomes structurally unstable and this instability leads to a time dependent state with realistic turbulent statistics that rapidly evolves toward a minimal representation of wall bounded shear turbulence in which the dynamics are limited to interaction of the streamwise mean flow with a single streamwise wave structure. In this naturally emergent minimal turbulence model the streamwise mean flow is supported by Reynolds stress torque organized from the perturbation field while the perturbation field is supported by the universal parametric non-normal growth process inherent to time dependent dynamical systems. This analysis shows how the roll/streak structure recruits supporting oblique waves from the background turbulence and how for sufficiently high levels of forced turbulence the interaction between these waves and the roll/streak can result in transition to and maintenance of a turbulent state.

Key Words: nonlinear dynamical systems; transition to turbulence; coherent structures; turbulent boundary layers

1. Introduction

Coherent structures are commonly observed in turbulent wall bounded shear flows in the atmosphere and in the laboratory as well as in simulations and these structures have long been the subject of both theoretical and practical interest. Understanding the dynamics of coherent structures is of theoretical interest because of the importance of these structures in the mechanism of turbulence transition and maintenance as well as in the transport of momentum and tracers. In addition coherent structure dynamics has practical implications for turbulence control and for improving parameterizations of turbulent heat and momentum transport. Coherent structures in planar wall bounded shear flows are generally recognized to arise from organization of convection if the flow is convectively unstable and from eddy/mean flow shear dynamics if it is neutrally stratified (Kuo 1963; Brown 1970, 1972; LeMone 1973, 1976; Etling & Brown 1993; Moeng & Sulivan 1994; Foster 1997; Bakas *et al.* 2001). Both observations and simulations confirm that the turbulent wall bounded shear flow, whether neutrally stratified or convectively unstable, is dominated by the universal structure of the coherent motions: streamwise roll vortices and associated high and low velocity streamwise streaks (Townsend 1956; Kline *et al.* 1967; LeMone 1973; Etling & Brown 1993; Moeng & Sulivan 1994; Komminaho *et al.* 1996; Lin *et al.* 1996; Hutchins & Marusic 2007; Adrian 2007; Wu & Moin 2009). Despite differences in scale, Reynolds number, and boundary conditions, the coherent structures in neutral planetary boundary layer (PBL) turbulence are essentially identical to those found in turbulent laboratory shear flows suggesting a commonality in the mechanism underlying the formation of the roll/streak/oblique wave complex in turbulent wall bounded shear flows.

There is an important difference between the turbulence in the neutrally stratified atmospheric PBL and that in DNS simulations and laboratory experiments: while the boundary in a simulation can be assumed analytically smooth and that in a laboratory experiment can be carefully prepared and the level of free stream turbulence can be controlled this is not the case in real world wall bounded shear flows. In fact turbulence in the PBL is strongly mechanically forced by imperfections in the boundaries and for this reason the surface roughness is a primary variable in PBL turbulence.

The appearance of the same roll/streak structure in shear flow under quite different physical conditions could be ascribed to its being the most amplified outcome of an initial value problem or alternatively to the mechanism of turbulence generating and supporting that structure. These are fundamentally related explanations because both the growth and maintenance mechanism exploit the same most robustly growing nonmodal entity in shear flow, the roll/streak. In the context of laboratory shear flows three dimensional perturbations in the form of a roll/streak structure were associated early with the robust nonmodal lift-up growth mechanism (Ellingsen & Palm 1975; Landahl 1980), and this insight was advanced by the recognition of the importance of dynamical operator non-normality and associated transient growth processes (Schmid & Henningson 2001). These analyses confirmed that the optimally growing three dimensional structures are cross-stream/spanwise rolls and associated streamwise streaks related to the linear lift up mechanism. The remarkable convected coordinate solutions for perturbation growth in unbounded shear flow (Kelvin 1887) allow closed form solution for the scale independent structures producing optimal growth in three dimensional shear flow (Farrell & Ioannou 1993*a*,*b*). These closed form optimal solutions in unbounded shear flow confirm the result found numerically in bounded shear flows that for sufficiently long optimizing times streamwise rolls produce optimal energy growth while for short optimizing times the optimal perturbations are oblique wave structures that synergistically exploit both the two dimensional shear and the three dimensional lift up mechanisms producing obliques waves oriented at an angle of approximately 60 degrees from the spanwise direction.

And indeed, the roll/streak and oblique accompanying wave structure complex that is predicted to produce optimal growth by analysis of non-normal perturbation dynamics of shear flows has been convincingly seen in both observations and simulations (Klebanoff *et al.* 1962; Schoppa & Hussain 2000; Adrian 2007; Hutchins & Marusic 2007; Wu & Moin 2009) and shown to be essentially related to the non-normality of shear flow dynamics (Kim & Lim 2000; Schoppa & Hussain 2002).

Although the mechanism of non-normal growth has been clarified, and its importance in bypass transition and maintenance of turbulence is widely accepted, the route by which non-normality leads to formation of the roll/streak structure in turbulent wall bounded shear flows and the part played by this coherent structure in the transition to turbulence and maintenance of the turbulent state remains to be determined.

The most direct mechanism exploiting non-normality to form roll/streak structures is introduction of an optimal or near optimal perturbation into the flow, perhaps by using a trip or other device. A related approach is to stochastically force the flow, with stochastic forcing regarded as modeling surface roughness and other external forcing (Farrell & Ioannou 1993*e*,*d*, 1994, 1998*a*,*b*; Bamieh & Dahleh 2001; Jovanovic & Bamieh 2005; Hoepffner & Brandt 2008). In these models the roll/streak structure is envisioned to arise from chance occurrence of optimal or near optimal perturbations in the stochastic forcing (Bamieh & Dahleh 2001; Hwang & Cossu 2010*a*; Gayme *et al.* 2010; Hwang & Cossu 2010*b*). These mechanisms exploit the linear non-normal growth process directly. However, the ubiquity of streak formation suggests, as argued by Schoppa & Hussain (2000), that some form of instability process also underlies the formation of streaks, that this instability involves an intrinsic association between the roll/streak structure and associated oblique waves and vortices, and that this three dimensional instability must differ qualitatively from the familiar laminar shear flow instability.

Although streamwise inhomogeneity in flat plate boundary layers complicates comparison with streamwise homogeneous wall bounded shear flow these results are nevertheless suggestive and from a comparison of experiment with simulation Andersson *et al.* (1999) conclude that in the case of a flat plate boundary the evidence "..corresponds to some fundamental mode triggered in the flat-plate boundary layer when subjected to high enough levels of free-stream turbulence..". In the work of Andersson *et al.* (1999) and Luchini (2000) a mode is simulated by placing at the leading edge of a flat plate a zero frequency optimal forcing that excites a roll/streak structure growing for a distance downstream before decaying. A sequence of these forced modes is shown to have many features in common with the results of experiments by Westin *et al.* (1994) and Matsubara & Alfredsson (2001) which show linear downstream growth of the square streak velocity.

An alternative nonlinear mechanism producing downstream growing roll/streak structures involves a streamwise average torque produced by interaction of discrete oblique waves and/or T-S waves. This mechanism was investigated by Benney (1960, 1984); Jang *et al.* (1986); Schmid & Henningson (1992); Reddy *et al.* (1998). Exponential instability mechanisms include centrifugal instability (Brown & Thomas 1977; Hall 1990) and the Craik-Leibovich instability (Phillips *et al.* 1996).

The cross-stream/spanwise roll structure provides a powerful mechanism for forming streamwise streaks in shear flows whether it is forced linearly by an initial condition or nonlinearly by an imposed set of oblique waves. However, in the absence of feedback from the streak back to the roll this powerful streak formation mechanism does not result in exponential instability although because of the large streak growth produced by a cross-stream/spanwise roll perturbation, placing even a very weak coupling of the streak to the roll, such as by a small spanwise frame rotation, produces destabi-

lization (Komminaho *et al.* 1996; Farrell & Ioannou 2008*a*). Turbulent Reynolds stress provides an alternative mechanism for producing the feedback between the streak and roll needed to destabilize the roll/streak structure. Indeed, if we observe a turbulent shear flow in the cross-stream/spanwise plane at a fixed streamwise location we see that at any instant there is a substantial torque from Reynolds stress divergence forcing cross-stream/spanwise rolls. The problem is that this torque is not systematic and so it vanishes in temporal or streamwise average. However, in the presence of a perturbation streak the symmetry in the spanwise direction is broken and the torque from Reynolds stress divergence becomes organized to produce the positive feedback between the streak and roll required to destabilize this structure by continuously and coherently exploiting the powerful non-normal roll/streak amplification mechanism. The existence of this mechanism for destabilizing the roll/streak structure in turbulence makes it likely that some dynamical perturbation complex exists to exploit it. In this work we prove by construction that this is so by deriving a system of equations eigenanalysis of which reveals the unstable roll/streak/turbulence structure. This emergent instability can be understood as a streak growth mechanism in which existing mechanically forced turbulence is organized by the perturbation streak into oblique waves that force the cross-stream/spanwise roll by inducing a Reynolds stress torque linearly proportional to streak amplitude thereby producing an exponential instability of the combined roll/streak/turbulence complex. This instability differs from optimal growing structures in that the roll/streak is forced by its associated oblique waves. However, these mechanisms necessarily occur together in forced turbulence so that a streak with structure close to an eigenmode of the interaction dynamics recruits oblique waves that cause it to grow suggesting a path by which an optimal initial condition can be effectively transformed into a mode.

Constructing a theory for this cooperative instability requires finding a method of analysis analogous to the method of modes for laminar flow instability, but applicable to this turbulence/mean flow interaction instability. Specifically, analysis of the cooperative instability of the roll/streak/turbulence complex is facilitated by constructing a dynamical system for evolving a physically accurate approximation of the statistical mean turbulent state. We refer to this dynamical system as the stochastic structural stability theory (SSST) system. This method for analyzing the dynamics of a turbulent system was developed to study the phenomenon of spontaneous jet formation at global scale in planetary atmospheres (Farrell & Ioannou 2003, 2007, 2008*a*) and has also been applied to the problem of spontaneous jet formation from drift wave turbulence in magnetic fusion devices (Farrell & Ioannou 2009). In SSST the turbulence is simulated using a stochastic turbulence model (STM) in which forcing by both extrinsic excitation and nonlinear scattering are parameterized as stochastic (Farrell & Ioannou 1993*c*, 1996*a*; DelSole & Farrell 1996; Bamieh & Dahleh 2001; DelSole 2004; Gayme *et al.* 2010). The STM provides an evolution equation for the quadratic statistics of the turbulent eddy field associated with a mean flow. In the STM the eddy field is expressed in terms of a covariance matrix from which the Gaussian probability density function approximation for the turbulence variance and quadratic fluxes can be obtained. Coupling a time dependent STM to an evolution equation for the streamwise mean roll/streak/shear complex produces a nonlinear dynamical system for the co-evolution of the roll/streak/shear and the self-consistent quadratic statistics of its associated turbulence: this is the SSST system.

The SSST equations incorporate a stochastic parameterization but these equations are themselves deterministic and autonomous with dependent variables the streamwise mean roll/streak/shear complex and the streamwise mean covariance of the turbulence. The perspective on shear flow stability provided by these equations differs from the more

familiar perspective based on perturbation stability of stationary laminar flows. In fact, the primary perturbation instability in SSST has no counterpart in the stability theory of laminar flow; it is the cooperative instability described above in which the evolving roll/streak/shear complex organizes the background turbulence covariance to produce flux divergences configured to amplify the roll/streak/shear complex leading to an emergent coupled roll/streak/shear plus turbulence instability that typically does not involve perturbation instability of the streak. We refer to this cooperative instability as structural instability to distinguish it from laminar flow instability such as would be associated with inflection of the streamwise velocity profile. The structural instability reveals constructively how turbulence is organized naturally by the streak to support the roll/streak structure. The SSST equations incorporate the nonlinear streamwise mean dynamics of the coupled roll/streak/shear plus turbulence dynamics and may, over a range of parameter values, produce nonlinear equilibration of the emergent roll/streak/shear complex and its consistent turbulence field at finite amplitude.

While the solution trajectory of an initially unstable SSST state may converge for a range of parameters to a fixed point representing a state of balance among the mean flow forcing and advection, the turbulent Reynolds stress divergence, and the damping; these finite amplitude equilibria ultimately lose structural stability as a function of the parameters and this instability in the case of wall bounded shear flows leads to a time-dependent solution.

In this work we concentrate first on how the growth of roll/streak structures in wall bounded shear flows is related to the interaction between the forced turbulence and the streamwise mean flow. We show that this interaction amplifies appropriately configured roll/streak structures and over a range of parameters produces sufficient amplification to destabilize these structures. We then show how these instabilities equilibrate nonlinearly at finite amplitude to maintain a statistically stable mean roll/streak/turbulence structure. One example of such a statistically homogeneously forced shear flow occurs over a rough ocean or the salt flats of Western Utah (Hutchins & Marusic 2007) in which turbulence is continuously forced externally by e.g. surface roughness. A related phenomena occurs in developing flat plate boundary layers in which turbulence entering from upstream forces spatially growing roll/streak structures (Westin *et al.* 1994; Wu & Moin 2009), although thorough analysis of this problem requires a spatial rather than temporal stability analysis (Andersson *et al.* 1999; Luchini 2000).

The eddy/mean flow instability that we are analyzing necessarily interacts with developing optimal excitations present in the forced turbulence facilitated by their sharing the same roll/streak structure (Berlin & Henningson 1999; Brandt & Henningson 2002). Given that optimal roll/streak structures are present, the SSST analysis reveals how these growing structures naturally recruit oblique waves and how these oblique waves ultimately promote the roll/streak structure to turbulence. This transition of an optimal initial condition into a mode by its recruitment of the background turbulence, which we will demonstrate by example, provides a suggestive route toward explaining similar phenomena seen in experiments in which the growth of an optimal initial condition is continued at essentially its initial growth rate far beyond the point at which it should begin to decay and continuing until transition occurs (Westin *et al.* 1994; Matsubara & Alfredsson 2001).

We believe that the mechanically forced turbulence regime, is common in naturally occurring boundary bounded shear flows. However, at sufficiently high turbulence intensity or Reynolds number a transitional structural instability leads to a distinct dynamical regime in which the mechanical forcing is no longer needed to maintain the turbulence

and the system transitions to a self-sustaining turbulent state. The self-sustaining state is examined in the second part of this paper.

We turn now to relating SSST equilibria and their structural instability to transition and maintenance of this self-sustaining turbulent state. While it is straightforward to show that non-normality is responsible for maintaining perturbation variance in shear flow turbulence (Drazin & Reid 1981; Henningson & Reddy 1994; Henningson 1996), nonlinearity is also necessary to sustain this non-normal growth (Kim & Lim 2000) and the exact mechanism by which the primary non-normal structures, the roll/streak and oblique waves, interact nonlinearly to sustain the turbulent state remains to be determined.

Among mechanisms advanced to explain systematic organization of the roll/streak structure in turbulence, Hamilton *et al.* (1995); Waleffe (1997); Jimenez & Pinelli (1999) proposed organization through a self-sustained cycle of roll/streak growth and decay supported by inflectional instability of the streak. The vortex-wave theory (Hall & Smith 1991; Hall & Sherwin 2010) proposed the self-sustained process arises from mean torques associated with mode critical layers. Alternatively, organization of roll/streak structure has been associated with episodic occurrence of exact non-linear unstable solutions with roll/streak structure (Waleffe 2003; Gibson *et al.* 2008).

We find that SSST equilibrium roll/streak structures are no longer supported when the forced turbulence or the Reynolds number exceeds a threshold and a secondary structural instability ensues leading to a time dependent state. This time dependent SSST state evolves toward a minimal self-sustaining process in which perturbation variance is maintained by a parametric non-normal time dependent instability mechanism (Farrell & Ioannou 1996*b*, 1999; Poulin *et al.* 2003; Pedlosky & Thomson 2003; Farrell & Ioannou 2008*b*; Poulin *et al.* 2010). In this evolution a dominant perturbation from the streamwise mean emerges naturally as a result of a process of purification of structure that occurs generically in time dependent systems (Farrell & Ioannou 1996*b*, 1999, 2002) and that is related closely to emergence of a dominant Lyapunov vector in time dependent linear systems. This self-sustaining process is similar to that advanced by Hamilton *et al.* (1995) for interpreting the self-sustained process in a minimal channel in being supported by nonlinear forcing of the optimally growing non-normal roll/streak structure but differs in not being related to inflectional instability. Emergence of a dominant structure by the purification process naturally reduces the dimension of the minimal realization further and suggests that application of continuation methods to this system may allow us to identify in future work embedded unstable closed orbits in this reduced phase space providing a bridge to recent results implicating exact coherent structures in transition and maintenance of turbulent flows.

We begin by reviewing the physical ideas behind roll forcing by perturbations, then derive the SSST system in the context of wall bounded shear flow, and finally apply this system to the problems of forced and free shear turbulence.

2. Mechanism of mean streamwise vortex forcing by turbulence

Consider perturbation Reynolds stresses $\overline{u_i u_j}$, where u_i is one of the three components of the eddy velocity field, u in the streamwise, x, direction; v in the cross-stream, y, direction; and w in the spanwise, z, direction. Here and in the sequel an overline denotes a streamwise mean. The streamwise mean force in the z direction is

$$F_z = -\frac{\partial \rho \overline{vw}}{\partial y} - \frac{\partial \rho \overline{w^2}}{\partial z}$$

and the streamwise mean force in the y direction is:

$$F_y = -\frac{\partial \rho \overline{vw}}{\partial z} - \frac{\partial \rho \overline{v^2}}{\partial y} \ .$$

Consequently the x component of the streamwise mean torque is:

$$\begin{aligned} G_x &= \frac{\partial F_z}{\partial y} - \frac{\partial F_y}{\partial z} \\ &= \left(\frac{\partial^2}{\partial z^2} - \frac{\partial^2}{\partial y^2} \right) \rho \overline{vw} + \ \frac{\partial^2}{\partial y \partial z} \rho \left(\overline{v^2} - \overline{w^2} \right) \ . \end{aligned}$$

In order to appreciate the generality of the Reynolds stress torque mechanism consider the simple perturbation field in an unbounded domain:

$$u = \mathrm{Re}\left(u_0 \cos(mz) \mathrm{e}^{\mathrm{i}kx}\right) \ , \ v = \mathrm{Re}\left(v_0 \cos(mz) \mathrm{e}^{\mathrm{i}kx}\right) \ , \ w = \mathrm{Re}\left(w_0 \sin(mz) \mathrm{e}^{\mathrm{i}kx}\right) \ , \quad (2.1)$$

with $\mathrm{i}ku_0 + mw_0 = 0$ to enforce nondivergence. This perturbation field consists of a pair of oblique waves in the (x, z) plane with wave vectors $(k, \pm m)$ inclined at an angle in the spanwise/streamwise plane of $\Theta = \pm \tan^{-1}(m/k)$ from the x direction. The Reynolds stress:

$$\overline{vw} = \frac{1}{4} \mathrm{Re}(v_0 w_0^*) \sin(2mz) \ ,$$

in which $*$ denotes complex conjugation, induces a spanwise (z) dependent mean force $F_y(z)$ in the y direction inducing the mean torque in the x direction:

$$G_x = -\rho m^2 \mathrm{Re}(v_0 w_0^*) \sin(2mz) \ . \quad (2.2)$$

The torque has double the spanwise wavenumber of the perturbation field and vanishes when $m = 0$ in which case the angle of obliquity is $\Theta = 0$. The torque also vanishes for $k = 0$ for which $\Theta = 90^0$ showing that streamwise roll perturbations as well as pure cross-stream Orr perturbations do not produce a mean torque. Streamwise mean torque is associated with oblique waves and it is immediate from (2.2) that for given perturbation energy and total horizontal wavenumber, $k^2 + m^2$, the torque is maximized at the intermediate angle of obliquity $\Theta = 54.7^0$.

Similar torques are produced by a pair of evolving oblique waves in an unbounded constant shear flow, $U = \alpha y$ with initial velocities:

$$u = \mathrm{Re}\left(u_0 \cos(mz) \mathrm{e}^{\mathrm{i}kx + \mathrm{i}ly}\right) \ , \ v = \mathrm{Re}\left(v_0 \cos(mz) \mathrm{e}^{\mathrm{i}kx + \mathrm{i}ly}\right) \ , \ w = \mathrm{Re}\left(w_0 \sin(mz) \mathrm{e}^{\mathrm{i}kx + \mathrm{i}ly}\right) \ . \quad (2.3)$$

The resulting time dependent torque is shown in the Appendix to be:

$$G_x = -\rho \frac{m^2 K^2(0)}{K^2(t)} \mathrm{Re}(v_0 w_0^*) \ \sin(2mz) \ ,$$

where $K^2(t) = k^2 + (l - \alpha k t)^2 + m^2$ is the total wavenumber at time t.

This initial wave produces coherent mean streamwise torque over its lifecycle maximizing at the same obliquity angle, $\Theta = 54.7^0$, as in the absence of shear, as shown in Fig. 1. It can also be shown using this closed form solution that energy growth over short time intervals is maximized for oblique perturbations (Farrell & Ioannou 1993*a*,*b*) with $\Theta = 63^0$ which is close to the orientation of the oblique waves maximizing the induced torque. We therefore anticipate that perturbations with angle of obliquity near the energy optimization value, $\Theta = 63^0$, will also be the main contributors to torque generation in shear flow. However, the fact that oblique waves give rise to coherent streamwise torques

does not explain the presence of coherent streamwise vortices when the perturbation field statistics are spanwise statistically uniform.

In the investigations by Benney (1960); Jang *et al.* (1986); Hall & Smith (1991); Schmid & Henningson (1992); Hall & Sherwin (2010) spanwise symmetry is broken by introducing a specific mix of TS waves and/or oblique perturbations. In the presence of spanwise homogeneous turbulence streamwise mean torques can also arise if the spanwise independence of the streamwise mean flow is broken. Remarkably, the slightest spanwise structure in the streamwise flow affects the turbulence in such a way as to induce coherent streamwise mean torques.

We demonstrate this tendency by calculating the induced streamwise torque that results when spanwise homogeneous turbulence interacts with a Couette flow which has been perturbed by the spanwise dependent streamwise flow

$$\delta U = \epsilon \cos(\pi y/(2L_y)) \cos(2\pi z/L_z) \ , \quad \text{with} \quad \epsilon << 1.$$

Reynold's stresses are obtained using the STM that will be described in section 4 (cf. Farrell & Ioannou (1993*e*); Bamieh & Dahleh (2001); Jovanovic & Bamieh (2005); Hoepffner & Brandt (2008)). The result, as shown in Fig. 2, is a coherent torque collocated with the streamwise perturbation that arises because the eddy field is modified by the streak perturbation. Such a coherent torque and its associated eddy field would be naturally recruited by a roll/streak structure excited by an initial condition and this coherent torque would in turn modify the mean flow which would then further organize the turbulence. However, most streamwise flow perturbations organize torques that do not exactly amplify the mean flow perturbation that produced them, as is the case for the perturbation in Fig. 2. Exponential modal growth of a streamwise mean flow and its associated eddy field would result if the mean flow perturbation organizes precisely the eddy field required for its amplification. We will show constructively in the next sections by using eigenanalysis that such cooperative unstable structures exist. An initial condition excited roll/streak structure would then be expected to tend toward the structure of a nearby eigenmode and we will show by example this interaction between a growing roll/streak structure and its nearby SSST eigenfunction..

3. Formulation of the composite roll/streak/turbulence dynamics

We decompose the velocity field into streamwise mean components (indicated uppercase) and perturbations (indicated lowercase) so that the total streamwise velocity in the x direction is $U(y,z,t) + u(x,y,z,t)$, the cross-stream velocity in the y direction is $V(y,z,t) + v(x,y,z,t)$, and the spanwise velocity in the z direction is $W(y,z,t) + w(x,y,z,t)$. The flow is confined to the channel $|y| \leqslant 1$, $|z| \leqslant L_z/2$ and the Reynolds number, R, is based on the half cross-stream channel distance $L_y = 1$. With constant velocity channel walls forcing a Couette flow as a laminar equilibrium the boundary conditions are $U(\pm 1,z,t) = \pm 1$, $V(\pm 1,z,t) = W(\pm 1,z,t) = 0$ and $u(x,\pm 1,z,t) = v(x,\pm 1,z,t) = w(x,\pm 1,z,t) = 0$ which imply that the normal vorticity $\eta = \partial_z u - \partial_x w$ satisfies the boundary condition $\eta(x,\pm 1,z,t) = 0$ and from continuity, $v_y(x,\pm 1,z,t) = 0$. Periodic boundary conditions are imposed in the spanwise direction and in addition the mean W flow is required to satisfy:

$$\int_{-L_z/2}^{L_z/2} W(y,z)dz = 0$$

so that no spanwise mean spanwise flow develops.

We write equations for the perturbations from the streamwise mean flow, $U(z,y,t)$,

neglecting the small spanwise and cross-stream mean flows, as it can be verified that $||V||, ||W|| << ||U||$. The perturbation equations can be reduced, following steps similar to those used in the derivation of the Orr-Sommerfeld and Squire system (Schmid & Henningson 2001), to two equations in the normal velocity, v, and normal vorticity, η:

$$v_t + \Delta^{-1}(U\Delta v_x + U_{zz}v_x + 2U_z v_{xz} - U_{yy}v_x - 2U_z w_{xy} - 2U_{yz}w_x - \Delta\Delta v/R) = F_v \ , \tag{3.1a}$$

$$\eta_t + U\eta_x - U_z v_y + U_{yz}v + U_y v_z + U_{zz}w - \Delta\eta/R = F_\eta \ . \tag{3.1b}$$

where Δ^{-1} is the inverse of the Laplacian, $\Delta \equiv \partial^2_{xx} + \partial^2_{yy} + \partial^2_{zz}$. On the RHS F_v and F_η represent deviations of the perturbation-perturbation advection from its streamwise average, together with forcing from surface roughness and other external sources. Parameterization of these terms will be specified in the next section.

The spanwise and streamwise velocity expressed in terms of the variables v and η are:

$$\Delta_h w = -v_{yz} - \eta_x \quad , \quad \Delta_h u = -v_{yx} + \eta_z, \tag{3.2}$$

in which $\Delta_h \equiv \partial^2_{xx} + \partial^2_{zz}$ denotes the horizontal Laplacian.

The mean streamwise flow, U, evolves according to

$$U_t = -(UV + \overline{uv})_y - (UW + \overline{uw})_z + \Delta U/R \ . \tag{3.3}$$

The mean streamwise flow is maintained against dissipation by the streamwise component of the force from the eddy Reynolds stresses and by the acceleration induced by the mean roll circulation $-(UV)_y - (UW)_z$ which can be written equivalently as $-U_y V - U_z W$. In spanwise independent flows this term reduces to $-U_y V$ and represents the familiar lift up mechanism. In order to evolve the mean streamwise flow the eddy Reynolds stresses and the fields V and W associated with the roll circulation are required.

The streamwise mean cross-stream and spanwise velocities; V and W respectively, can be obtained from the mean streamfunction $\Psi(y, z, t)$:

$$V = -\Psi_z \quad , \quad W = \Psi_y \ , \tag{3.4}$$

which evolves according to the mean streamwise vorticity equation:

$$\Delta\Psi_t = (VW + \overline{vw})_{zz} - (VW + \overline{vw})_{yy} - (W^2 - V^2 + \overline{w^2} - \overline{v^2})_{yz} + \Delta\Delta\Psi/R \ . \tag{3.5}$$

The streamwise mean vortex is forced by the torque from perturbation Reynolds stresses as discussed in the previous section. This eddy torque maintains the streamwise mean vorticity against dissipation while the mean cross-stream and spanwise velocities only advect mean streamwise vorticity.

Equations (3.1*a*, 3.1*b*, 3.3, 3.5) comprise the roll/streak/turbulence dynamics. In the absence of forcing this system has as a stable equilibrium solution only the Couette flow $U = y$, $V = W = 0$. In the presence of forcing the combined roll/streak/turbulence dynamics includes the mean Reynolds stress from the perturbation field governed by (3.1*a*, 3.1*b*, 3.3, 3.5) giving rise to new equilibria. We next show how SSST can be used to find these new stable equilibria.

4. The SSST system governing roll/streak/turbulence dynamics

The SSST system includes the three components of the streamwise mean flow (3.3, 3.5), and the ensemble mean Reynolds stress from the perturbations (3.1*a*, 3.1*b*). Stochastic excitation is used in the perturbation equations to parameterize both the exogenous forcing and the endogenous scattering by eddy-eddy interactions. The perturbation equations

with this parameterization comprise the Stochastic Turbulence Model (STM). The STM provides accurate eddy structure at the energetic scales in strongly sheared flow because the dynamics associated with the non-normal linear operator dominates in determining the perturbation structure (Farrell & Ioannou 1998*b*; Laval *et al.* 2003). This parameterization has been widely used to describe the dynamics of turbulence in channel flows (Farrell & Ioannou 1993*e*, 1994, 1998*a*; Bamieh & Dahleh 2001; Jovanovic & Bamieh 2005; Hoepffner & Brandt 2008; Hwang & Cossu 2010*a*; Gayme *et al.* 2010) and has also been instrumental in advancing robust control of channel flow turbulence (Farrell & Ioannou 1998*b*; Bewley & Liu 1998; Kim & Bewley 2007; Hogberg *et al.* 2003*a*,*b*). The STM has also been verified to determine with great accuracy the eddy structure of the midlatitude atmosphere (Farrell & Ioannou 1995; DelSole & Farrell 1996; DelSole 1996; Whitaker & Sardeshmukh 1998; Zhang & Held 1999; DelSole 2001, 2004).

We use Fourier expansion in x for the perturbations that deviate from the streamwise mean:

$$v = \sum_k \hat{v}_k(y,z,t)\mathrm{e}^{\mathrm{i}kx} \ , \ \eta = \sum_k \hat{\eta}_k(y,z,t)\mathrm{e}^{\mathrm{i}kx} \ , \tag{4.1}$$

in which the $k = 0$ streamwise wavenumber is excluded. We discretize the perturbation equations (3.1*a*, 3.1*b*) in y and z so that the state is prescribed for each Fourier component by the cross-stream velocity and vorticity as $\hat{\boldsymbol{\phi}}_k = [\hat{\boldsymbol{v}}_k, \hat{\boldsymbol{\eta}}_k]^T$ on a $y-z$ grid. All quadratic perturbation quantities including streamwise mean Reynolds stresses can be obtained from the streamwise mean covariance matrix of the perturbation state, $\mathsf{C}_k = \overline{\hat{\boldsymbol{\phi}}_k \hat{\boldsymbol{\phi}}_k^\dagger}$ (with $\dagger$ denoting Hermitian transpose). Under the ergodic assumption this streamwise mean covariance is the same as the ensemble mean covariance $\mathsf{C}_k = < \hat{\boldsymbol{\phi}}_k \hat{\boldsymbol{\phi}}_k^\dagger >$ (in this expression $< \cdot >$ denotes ensemble averaging and the subscript indicates that the statistics are those of the eddy field components with that streamwise wavenumber). The ergodic assumption is employed because the ensemble covariance can be readily calculated.

We take an excitation in (3.1*a*, 3.1*b*) that is delta correlated in time and of the general form:

$$\begin{pmatrix} \boldsymbol{F}_v \\ \boldsymbol{F}_\eta \end{pmatrix} = \mathsf{F}\boldsymbol{\xi}$$

where $\boldsymbol{\xi}(t)$ is a normally distributed independent random column vectors of length equal to twice the number of discretization points, that satisfies:

$$< \xi_i(t)\xi_j(s) >= \delta_{ij}\delta(t-s),$$

with the structure matrix F determining the spatial coherence of the forcing at streamwise wavenumber k through its covariance Q_k:

$$\mathsf{Q}_k = \mathsf{F}\mathsf{F}^\dagger \ . \tag{4.2}$$

The qualitative features of the SSST dynamics are insensitive to the structure of the forcing reflected in, Q_k, so long as it excites the most energetic structures. The reason is the high non-normality of the perturbation operator which leads to strong amplification of a few optimal structures which dominate the perturbation field.

We take Q_k to be proportional to M_k^{-1}, where M_k is the metric that determines the perturbation kinetic energy at streamwise wavenumber k through the inner product:

$$E_k = \hat{\boldsymbol{\phi}}_k^\dagger \mathsf{M}_k \hat{\boldsymbol{\phi}}_k \ . \tag{4.3}$$

This forcing covariance excites the system so that each degree of freedom receives equal

energy. The energy metric is given by

$$M_k = \frac{1}{4}\left(L_u^{k\dagger}L_u^k + L_v^{k\dagger}L_v^k + L_w^{k\dagger}L_w^k\right) \ , \tag{4.4}$$

where $\hat{\boldsymbol{u}}_k = L_u^k\hat{\boldsymbol{\phi}}_k$, $\hat{\boldsymbol{v}}_k = L_v^k\hat{\boldsymbol{\phi}}_k$, and $\hat{\boldsymbol{w}}_k = L_w^k\hat{\boldsymbol{\phi}}_k$. Explicitly, the linear operator L_v^k is the projection,

$$L_v^k = [I \ \ 0] \ , \tag{4.5}$$

while the two other linear operators are obtained using Equation (3.2):

$$L_u^k = \begin{pmatrix} -\mathrm{i}k\Delta_h^{-1}\partial_y & 0 \\ 0 & -\Delta_h^{-1}\partial_z \end{pmatrix} \ , \ L_w^k = \begin{pmatrix} -\Delta_h^{-1}\partial_{yz}^2 & 0 \\ 0 & -\mathrm{i}k\Delta_h^{-1} \end{pmatrix} \ . \tag{4.6}$$

The covariance evolves according to the deterministic Lyapunov equation (Farrell & Ioannou 1996*a*):

$$\frac{\mathrm{d}C_k}{\mathrm{d}t} \ = \ A_k(U)C_k \ + C_kA_k^\dagger(U) \ + \ f^2Q_k \ , \tag{4.7}$$

in which f^2 is an amplitude factor and $A_k(U)$ is the linear operator in (3.1*a*, 3.1*b*) which depends on the streamwise flow $U(y,z,t)$. In matrix form the operator A_k in (4.7) is:

$$A_k(U) = \begin{pmatrix} L_{OS} & L_{C_1} \\ L_{C_2} & L_{SQ} \end{pmatrix} \ , \tag{4.8}$$

with

$$L_{OS} = \Delta^{-1}\left(-\mathrm{i}kU\Delta + \mathrm{i}k(U_{yy}-U_{zz}) - 2\mathrm{i}kU_z\partial_z - 2\mathrm{i}k(U_z\partial_{yyz}^3 + U_{yz}\partial_{yz}^2)\Delta_h^{-1} + \Delta^2/R\right), \tag{4.9a}$$

$$L_{C_1} = 2k^2\Delta^{-1}\left(U_z\partial_y + U_{yz}\right)\Delta_h^{-1}, \tag{4.9b}$$

$$L_{C_2} = U_z\partial_y - U_y\partial_z - U_{yz} + U_{zz}\partial_{yz}^2\Delta_h^{-1}, \tag{4.9c}$$

$$L_{SQ} = -\mathrm{i}kU\Delta + \mathrm{i}kU_{zz}\Delta_h^{-1} + \Delta/R \tag{4.9d}$$

The covariances, C_k, evolved by (4.7) provides the Reynolds stresses for the mean flow equations (3.3, 3.5). For example, the Reynolds stress component $\overline{uv}$ is given by:

$$\overline{uv} = \frac{1}{2}\mathrm{Re}\left(\mathrm{diag}\left(\sum_{i=1}^{n} L_u^{k_i}C_{k_i}L_v^{k_i\dagger}\right)\right) \tag{4.10}$$

where diag denotes the matrix diagonal and n the number of streamwise harmonics. All the Reynolds stresses can be written similarly as linear functions of the covariance matrix and the streamwise mean equations (3.3, 3.5) can then be expressed concisely in the form:

$$\frac{\mathrm{d}\boldsymbol{\Gamma}}{\mathrm{d}t} = G(\boldsymbol{\Gamma}) + LC \tag{4.11}$$

where $\boldsymbol{\Gamma} \equiv [\boldsymbol{U}, \boldsymbol{\Psi}]^T$ denotes the streamwise mean flow, G a function of the mean flow that includes the dissipation and external forcing, $C = [C_{k_1}, \cdots, C_{k_n}]$ and LC is the forcing of the mean by the Reynolds stresses, with L a linear operator.

Equations [(4.7), (4.11)] comprise the SSST system for the roll/streak/turbulence dynamics:

$$\frac{\mathrm{d}C_k}{\mathrm{d}t} = \ A_k(P\boldsymbol{\Gamma})C_k \ + C_kA_k^\dagger(P\boldsymbol{\Gamma}) \ + \ f^2Q_k \ , \tag{4.12a}$$

$$\frac{\mathrm{d}\boldsymbol{\Gamma}}{\mathrm{d}t} = G(\boldsymbol{\Gamma}) + LC \ , \tag{4.12b}$$

with P the projection of $\mathbf{\Gamma}$ onto the mean streamwise flow so that $P\mathbf{\Gamma} = \boldsymbol{U}$. By defining the SSST state $\boldsymbol{\chi} = [C, \mathbf{\Gamma}]^T$ the SSST dynamics can be written concisely as:

$$\frac{\mathrm{d}\boldsymbol{\chi}}{\mathrm{d}t} = S(\boldsymbol{\chi}) \ . \tag{4.13}$$

The equilibrium states satisfy $S(\boldsymbol{\chi}_{eq}) = 0$.

Equation (4.13) constitutes a closed, deterministic, autonomous, nonlinear system for the co-evolution of the streamwise mean flow and the STM approximation to its consistent field of turbulent eddies. Although the effects of the turbulent fluxes are retained in this system, the fluctuations associated with turbulent eddy dynamics are suppressed so that the dynamics of turbulent eddy/mean flow interaction and particularly the equilibria arising from this interaction are revealed with clarity.

We remark on some qualitative properties of the SSST dynamics:

(a) The SSST system is globally stable and the attractor of the SSST system may be a fixed point, a limit cycle, or a chaotic attractor. Examples of each of these behaviors has been found in the SSST description of geophysical and plasma turbulence (Farrell & Ioannou 2003, 2008a, 2009).

(b) The SSST system trajectory is the trajectory of an approximation to the statistical mean state of the turbulence which evolves on the time scale of the mean flow.

(c) The SSST system introduces a new stability concept: the stability of an equilibrium between a mean flow and its consistent field of turbulence. If a mean flow is perturbation unstable (in the sense of Rayleigh) it is also structurally unstable (in the sense of SSST). However, the converse is not true and roll/streak structures can grow as a result of structural instability in a perturbation stable state.

5. Structural stability of the spanwise independent mean streamwise flow with imposed forcing

Assume that for a given forcing covariance, $f^2 Q_k$, the nonlinear equilibrium $\boldsymbol{\chi}_{eq} = [C_{eq}, \mathbf{\Gamma}_{eq}]^T$ of the SSST equations (4.12) has been determined. We can study its stability by linearizing the SSST system about this equilibrium. The perturbation equations take the form

$$\frac{\mathrm{d}\delta C_k}{\mathrm{d}t} = A_k(P\mathbf{\Gamma}_{eq})\delta C_k \ + \delta C_k A_k^\dagger(P\mathbf{\Gamma}_{eq}) \ + \ \delta A_k C_{keq} \ + C_{keq}\delta A_k^\dagger \ , \tag{5.1a}$$

$$\frac{\mathrm{d}\delta\mathbf{\Gamma}}{\mathrm{d}t} = \left.\frac{\partial G}{\partial \mathbf{\Gamma}}\right|_{\mathbf{\Gamma}_{eq}} \delta\mathbf{\Gamma} + L\delta C \ . \tag{5.1b}$$

where $\delta\mathbf{\Gamma} = [\delta\boldsymbol{U}, \delta\mathbf{\Psi}]^T$ is the perturbation to the mean flow and δA_k is the perturbation to the mean operator. This operator perturbation is produced by perturbation to the mean streamwise flow, $\delta\boldsymbol{U}$. Setting $\delta\boldsymbol{\chi} \equiv [\delta C, \delta\mathbf{\Gamma}]^T$ the perturbation equations can be written concisely as:

$$\frac{\mathrm{d}\delta\boldsymbol{\chi}}{\mathrm{d}t} = \mathcal{L}\delta\boldsymbol{\chi} \tag{5.2}$$

The linear operator $\mathcal{L} \equiv \partial S/\partial\boldsymbol{\chi}|_{\boldsymbol{\chi}_{eq}}$ depends on the equilibrium state $\boldsymbol{\chi}_{eq} = [C_{eq}, \mathbf{\Gamma}_{eq}]^T$ which in turn depends on the Reynolds number R, the channel geometry, the mean flow forcing, and the turbulence intensity through its dependence on $f^2 Q_k$. Eigenanalysis of the linear operator $\mathcal{L}$ determines the structural stability of this equilibrium roll/streak/turbulence complex. The familiar laminar Couette flow equilibrium $\mathbf{\Gamma}_{eq} = [\boldsymbol{U}_{eq} = \boldsymbol{y}, \ \mathbf{\Psi}_{eq} = 0]^T$ and $C_{eq} = 0$ is a solution of the SSST equations (4.12) in the

absence of forcing ($f = 0$). Because for $f = 0$ the eddy covariance vanishes, $\mathcal{C}_{eq} = 0$, the first of the perturbation SSST equations (5.1) reduces to an unforced Lyapunov equation which inherits the perturbation stability of Couette flow at all Reynolds numbers. The second equation is asymptotically unforced and clearly stable so in the absence of forcing the system (5.1) is structurally stable as well as perturbation stable. From this argument it is clear that structural instability of a flow that is perturbation stable in the sense of Rayleigh requires non-vanishing $\mathcal{C}_{eq}$ or equivalently non zero values of f.

In the presence of spanwise homogeneous forcing there is a class of spanwise independent equilibria $\mathbf{\Gamma}_{eq} = [\boldsymbol{U}_{eq}(y), \mathbf{\Psi}_{eq} = 0]^T$ with non vanishing $\mathcal{C}_{eq}$. In these equilibria the mean streamwise flow $U_{eq}(y)$ is maintained by a balance between diffusion and the component of Reynolds stress divergence $-(\overline{uv})_y$ in the inhomogeneous (cross-stream) direction. The equilibria are possible because all the Reynolds stresses are independent of z, and symmetry requires that $\overline{vw} = 0$. We will demonstrate that for sufficient high f these equilibria, while remaining perturbation stable, become structurally unstable with eigenfunctions having the structure of roll circulations with associated streaks.

For convenience the amplitude of the forcing, $\mathcal{Q}_k$, is chosen to maintain RMS perturbation velocity 1% of the mean Couette flow velocity when it is used to excite the Couette flow. When this excitation is introduced into the perturbation variance equation as $f^2\mathcal{Q}_k$ the adjustable amplitude, f, corresponds approximately to RMS perturbation velocity fluctuations as a percentage of the mean flow velocity. This follows because RMS perturbation velocity is very nearly linearly proportional to f prior to the bifurcation to roll /streak equilibria although deviating slightly as the profile deviates from the Couette with increasing f.

Consider the structural stability of the spanwise independent equilibrium flow $\mathbf{\Gamma}_{eq} = [\boldsymbol{U}_{eq}(y),\ \mathbf{\Psi}_{eq} = 0]^T$ in with $L_z/(2\pi) = 0.6$, $R = 400$ and perturbation wavenumber $k = 1.143$. The calculations were made with $N_y = 21$ and $N_z = 40$ points with convergence checked at double resolution. The power method was used to find the structure and growth rate of the fastest growing eigenmode of the $\mathcal{L}$ operator in (5.2) for the streamwise flow in equilibrium with increasing values of the forcing amplitude, f. These spanwise independent equilibria are stable for $f \leqslant f_c$ where $f_c = 5.82$. At f_c the spanwise independent equilibrium becomes unstable (while the streamwise mean flow remains perturbation stable) and new equilibria with roll/streak structure emerge. The most unstable eigenfunction with growth rate $\lambda = 0.014$ is shown in Fig. 5 . The eigenfunction comprises both a mean flow perturbation, $\delta\mathbf{\Gamma}$, and an eddy covariance perturbation, $\delta\mathcal{C}$. The Reynolds stresses associated with $\delta\mathcal{C}$ produce accelerations and torques in exact agreement with the mean flow perturbation, consistent with exponential modal instability When this eigenfunction is introduced into the nonlinear SSST system(4.13) it grows at first exponentially at rate $\lambda = 0.014$, as predicted by SSST theory, and then equilibrates to a steady finite amplitude roll/streak structure as can be seen in Fig. 6. The bifurcation diagram in Fig. 3 shows as a function of f the mean kinetic energy of the roll component, E_r, obtained by averaging $(V^2 + W^2)/2$ over the channel; and of the streak component, E_s, obtained by averaging $U_s^2/2$, where the streak perturbation is $U_s = U - [U]$ with $[U] = \int_0^{L_z} U dz/L_z$. The structure of corresponding mean streamwise velocity equilibria are shown in Fig. 4 for $f = 5,\ 6,\ 7.4,\ 8.4$. At $f_c = 5.82$ the structural instability of the spanwise independent equilibrium gives rise to spanwise dependent roll/streak equilibria. These roll/streak equilibria are structurally stable up to $f_u = 8.45$ at which point there is a second bifurcation where the equilibrium becomes structurally unstable while the flow retains perturbation stability.

The SSST interaction slows the decay of roll/streak eigenfunctions for $f < f_c$ but does

not cause growth and produce equilibration until $f > f_c$. There is likely to be a finite amplitude near optimal initial condition present in the forced turbulence to initiate the growth of the SSST mode so that the SSST interaction would be seen as an increase in growth rate of the evolving optimal for $f < f_c$ followed by equilibration for $f_c < f < f_u$ and transition for $f > f_u$ rather than as emergence of the optimal eigenmode from an infinitesimal precursor. A series of integrations of an optimal initial condition in the Couette channel flow in the presence of various values of forced turbulence, parameterized by f, are shown in Fig 7. The optimal initial condition is seen to recruit the turbulent eddy field to support and maintain itself producing equilibria and finally destabilization for $f > f_u$. By this interaction an optimal is effectively converted into an SSST mode.

We have chosen to use f as a bifurcation parameter but analogous bifurcation structure results if R is used instead. For example, with $f = 7$ the stable roll/streak equilibria exist for $370 < R < 450$ and bifurcate to a time dependent state for $R > 450$.

6. The structure of the roll/streak equilibria in the forced regime

The SSST analysis predicts roll/streak equilibria in the range $f_c < f < f_u$ with streak amplitude increasing with f (as shown in Fig. 4) but with spanwise average streamwise flows, $[U]$, departing only slightly from the Couette flow. Indicative of this forced regime is low viscous dissipation rate of the streamwise mean flow:

$$D = \frac{1}{R}\int_0^{L_z} dz \int_{-L_y}^{L_y} dy (U_y^2 + U_z^2 + V_y^2 + V_z^2 + W_y^2 + W_z^2) \ .$$

The ratio D/D_C, where D_C is the dissipation rate associated with Couette flow, for equilibria with $f_c < f < f_u$ is in the range $1 < D/D_C < 1.4$ while this ratio is of order 3 in the turbulent state. Such low dissipation rates are more consistent with laminar than turbulent flow.

The essentially laminar roll/streak equilibria shown in Fig. 4 have spanwise wavenumber 2. The spanwise length of the channel for the equilibrium at $f = 8.4$, shown in Fig. 6, is $90y^+$ for (the wall unit is defined as $y^+ \equiv 1/\sqrt{R[U_y]}$, where R is the Reynolds number and $[U_y]$ is the mean shear at the boundary) implying streak spacing $45y^+$ which is about half the $100y^+$ wall unit spacing found in turbulent boundary layers (Smith & Metzler 1983). However, it should be kept in mind that the wall unit is here calculated for an essentially laminar flow. In section 7 we show that this spacing agrees with observed streak spacing in laminar boundary layers before transition (Westin *et al.* 1994). We obtain the greater spacing observed in turbulent wall bounded shear flows for forcing amplitudes greater than f_u for which the solution becomes chaotic.

Consider the contribution of the mean flow and the eddies to maintaining the roll/streak structure (cf. Eq. (3.3,3.5)). The roll circulation is maintained by the eddy torque (cf. Fig. 9a,c) while the streak (cf. Fig. 9b, c) is maintained by the resulting streamwise roll circulation through the lift-up mechanism. The direct affect of the eddies is to damp the streak.

We turn now to the structure of the eddy field at equilibrium. Eddy structures can be ordered in energy by eigenanalysis of $\mathsf{M}^{1/2}\mathsf{C}\mathsf{M}^{1/2}$, where $\mathsf{M}^{1/2}$ denotes the square root of the energy metric given in (4.4). Eigenfunctions of $\mathsf{M}^{1/2}\mathsf{C}\mathsf{M}^{1/2}$ in descending order of eigenvalue define the empirical orthogonal function (EOF) decomposition of the eddy field. The percentage of the energy accounted for by the 40 gravest modes of the covariance is shown in Fig. 10 for $f = 5$, for which the flow is spanwise uniform, and also for $f = 6,\ 7.5,\ 8.4$. It is clear that the variance is spread over many structures but as f increases the first EOF dominates and its structure becomes a good representation

of the eddy structure. This dominant EOF for the equilibrium structure at $f = 8.4$ is shown in Fig. 11 to be characterized by sinuous oblique waves centered at the wings of the streak. This structure produces coherent torques that maintain the roll circulation. The dominant EOF is close in structure to the least stable mode of the flow which is shown in Fig. 12. Note however that this mode is robustly stable so it is maintained by excitation and non-normality, with the latter dominant. The large excitation of the mode is due to the non normal interaction between this mode and the other stable modes of the system as revealed by its optimal excitation structure which is its adjoint (Farrell 1988; Hill 1995; Farrell & Ioannou 1996*a*). The adjoint of the least stable mode in the energy inner product is shown in Fig. 13. An initial condition consisting of its adjoint excites the least stable mode at amplitude a factor 1900 greater than an initial condition consisting of the least stable mode itself so the mode arises out of stochastic forcing primarily due to excitation of its adjoint.

Because the excitation is white in energy and all modes are stable the structure of the eddy field can be understood by examining optimal structure evolution. The optimal perturbation that leads to the greatest growth in energy in 10 time units for the equilibrium at $f = 8.4$ consists of a pair of oblique waves located at the wings of the streak and is very close in structure to the the adjoint shown in Fig. 13. The energy growth of this optimal is also close to the energy growth of the adjoint of the least stable mode as shown in Fig. 14. Evolution of the maximum mean streamwise torque, G_x, induced by the Reynolds stress divergence of the optimal perturbation and the adjoint mode is also shown in Fig. 14. The spanwise streak serves to collocate the perturbation structures aligning them so that the spanwise Reynolds stress divergence produce torques in phase with the evolving roll. The energy evolution and the torque produced by the $t = 10$ optimal for the equilibrium with $f = 5$, for which there is no streak and therefore no systematic organization, is also shown to be substantial in Fig. 14 demonstrating the streamwise mean torque arises from collocation of the non-normally growing oblique waves, which are the short time optimals, rather than from the influence, other than collocation, of the streak structure itself.

7. Streak spacing in transitional boundary layers forced by free stream turbulence

A fully developed turbulent boundary layer, such as that approximated by the Reynolds-Tiederman profile, is maintained by the ensemble of eddies in the boundary layer. It is commonly observed in turbulent boundary layers that spanwise streak spacing is approximately 100 y^+ with wall unit $y^+ \equiv \sqrt{\nu/([U_y])}$ and $[U_y]$ being evaluated at the boundary. As the boundary layer is itself approximately 50 y^+ in wall normal extent this spacing is consistent with a roll of unit aspect ratio confined to the boundary layer (Kim *et al.* 1987; Hutchins & Marusic 2007).

We have concentrated on the formation of streaks from forced turbulence in which the deviation of the mean boundary layer flow profile from the stationary Couette flow is small compared with that seen in fully turbulent boundary layers. In order to study streak spacing in a numerically resolved boundary layer example we maintain a Blasius profile stationary with an appropriate body force and subject it to supercritical forcing† $f > f_u$, and obtain the maximum growth rate of the structural instability as a function of spanwise wavenumber, m, of the unstable streak using the power method. Growth rate

† The parameter f is approximately equal to the Tu parameter used in the study of Westin *et al.* (1994).

of the most unstable SSST roll/streak eigenmodes at $f = 10$ in a Blasius boundary layer maintained at Reynolds number $R_{\delta^*} = 690$ (based on the displacement thickness $\delta^* = 1.72\sqrt{\nu x/U}$) as a function of obliquity angle and for spanwise quantized streak spacings are shown in Fig. 15. The maximum SSST instability occurs at the spanwise wavenumber corresponding to a spacing between low speed streaks of $\Delta z = 2.4\delta^*$, consistent with unit roll aspect ratio in agreement with observations (Westin *et al.* 1994). This maximum instability is associated with oblique waves with phase lines oriented at an angle $\Theta = \tan^{-1} m/k$ to the streamwise direction which is near the obliquity angle of 63^0 that characterizes short time optimals in shear flow (cf. section 2).

The structural instability of a Blasius boundary layer flow at $R_{\delta^*} = 600$ occurs at $f_u = 0.475$ for eddy structure at streamwise wavenumber $k = 1$. The emerging roll/streak complex does not equilibrate for any value $f > 0.475$ at this R_{δ^*} but rather transitions to a time dependent turbulent state. We now show the evolution of the roll/streak in a boundary layer flow which was initially in the form of a Blasius profile for various amplitudes of f. The initial perturbation is the $t = 40$ optimal roll perturbation with $k = 0$ and $m = 1.5$. For forcings $f < f_u$ the optimal ultimately decays, while for $f > f_u$ the optimal initial condition recruits the eddy field, grows and transitions to a time dependent state. The development of the square streak amplitude is shown in Fig. 16 for subcritical $f = 0.4$ and for supercritical $f = 0.75,\ 1$. The associated roll/streak structure is shown in Fig. 17 to lead to pronounced undulations of the mean flow which however are associated with modest changes in the cross-stream direction of the spanwise average streamwise mean flow $[U]$ until breakdown to the time dependent equilibrium is approached. A comparison of the developing mean flow and the normalized defect is shown in Fig. 18. Similar behavior is found in developing transitional boundary layers subjected to the same amplitudes of free stream turbulence (Westin *et al.* 1994; Matsubara & Alfredsson 2001).

8. The role of modes in the equilibration of the roll/streak

The SSST roll/streak equilibria in Couette flow for amplitudes near f_u are perturbation stable despite being inflected in the spanwise direction. The eigenvalues, σ, of the perturbation operators, A_k, are shown in Fig. 19 for the equilibria of Fig. 4. Note the emergence of a mode with frequency $\sigma_i = 0$ as f approaches f_u. This increasingly prominent perturbation structure is the sinuous mode that is commonly thought to be causally related to streak breakdown (Hamilton *et al.* 1995; Waleffe 1997; Reddy *et al.* 1998). However, at f_u the roll/streak flow is still robustly stable and the instability that occurs for $f > f_u$ is solely an instability of the cooperative turbulence/mean flow SSST dynamics associated with structural instability of the roll/streak equilibria.

We turn now to obtaining a clearer understanding of the dynamics underlying maintenance and loss of structural stability near the secondary bifurcation to time dependence at $f_u = 8.45$.

As f approaches f_u oblique non-normal wave perturbations dominate the eddy structures maintaining the mean roll and these produce a roll/streak equilibrium with highly inflected streaks (cf Fig. 4). In association with this inflection the primary inflectional mode, with structure shown in Fig. 12, approaches its stability boundary (cf Fig. 19d) while remaining stable. Consistent with drawing energy from the streak this mode produces strong downgradient Reynolds stresses that damp the streak while the Reynolds stress it produces forcing the roll circulation are relatively weak. In order to compare the relative contribution of the direct downgradient Reynolds stress due to the inflectional mode in damping the streak with the mode's indirect Reynolds stress effect in forcing

the roll circulation and thereby building the streak we impose a modification of the real part of the eigenvalue of the mode at equilibrium, specifically we set the damping rate of this mode equal to $0.9\sigma_{rE}$ (less damped) and $1.1\sigma_{rE}$ (more damped), and integrated forward the SSST equations in order to determine the mean flow tendency. When the mode is thus constrained to be less damped the perturbation energy increases and the associated roll circulation also increases, but the streak decreases because the enhanced downgradient fluxes by the less damped mode dominate over the increase in the streak induced by the roll circulation. The opposite happens when the mode is more damped, as shown in Fig. 20.

We conclude that this sinuous mode is the primary mechanism of streak stabilization at high forcing. However, as f rises above f_u the inflectional mode is no longer able to stabilize the streak and a second structural instability ensues in which the oblique waves further accelerate the roll/streak complex. However, the streak remains perturbation stable until a very high amplitude is reached at which point the mean flow becomes time dependent and aperiodic.

9. Transition to time dependence through loss of structural stability at f_u

The equilibrium at $f = f_u$ is robustly perturbation stable and the instability that occurs for $f > f_u$ is an instability of the cooperative turbulence/mean flow SSST dynamics. The perturbation energy, E_p, and roll energy, E_r, abruptly increase for value of f greater than the critical, f_u, as can be seen in Fig. 21. For values even marginally greater than f_u the flow eventually becomes chaotic and failure of continuation algorithms to find a stable equilibrium solution or limit cycle behavior indicates that the transition to chaos beyond f_u is through a saddle-node bifurcation†. Evolution of the eddy kinetic energy, roll energy, and streak energy for a typical transition to the chaotic state at $f = 10$ are shown in Fig. 21. The initial state is the roll/streak equilibrium that occurs at $f = f_u$ which is characterized by Couette flow normalized eddy kinetic energy 10%, normalized roll energy 2% and normalized streak energy 23%. At the level of forcing supported at $f = 10$ this initial state is modally stable but structurally unstable with consequent increase of the eddy kinetic energy, the roll kinetic energy and the streak energy with the last leading eventually to modal instability of the increasingly strongly spanwise inflected streak. Modal instability inception occurs at about $t = 200$ and this point is marked by a dotted line in Fig. 21. Beyond this point the flow transitions to an irregular time dependent state with energy input/dissipation parameters typical of turbulence as seen in Fig. 22.

10. Description of the turbulent state

This turbulent state is shown using snapshots of the streamwise mean flow and vectors of the spanwise/cross-stream flow in Fig. 23. At $t = 200$ the streamwise flow with streak spacing of about 50 wall units has become perturbation unstable and has transitioned to a time dependent state characterized by a roll streak structure with mean spacing of about 100 wall units that vacillates strongly in amplitude with the streak collapsing at times (panel for $t = 600$). The time and space scales characterizing the vacillation

† If we allow spanwise mean spanwise flow then there are weakly attracting slanted equilibrium states and limit cycle solutions for $f > f_u$ which bifurcate to a chaotic state at a higher value of f. However the behavior remains essentially the same.

regime are similar to those found in minimal channel simulations (Jimenez & Moin 1991; Hamilton *et al.* 1995) and the streak-spacing of about 100 wall units is also in agreement with observations (Smith & Metzler 1983; Komminaho *et al.* 1996). A typical time series of the time dependent roll/streak state shown in Fig. 24 exhibits trapping at irregular intervals of the turbulent state close to the laminar roll/streak state that is shown in Fig. 6.

When the channel flow has transitioned to the time dependent state for $f > f_u$, this state persists even if the forcing is removed by setting $f = 0$; although for $f < f_u$ this apparently chaotic state is transient being eventually terminated by laminarization to the stable equilibrium at the corresponding value of f. A time series showing this self-sustained state is shown in Fig. 25.

The spanwise and time mean streamwise flow for the turbulent state is shown in Fig. 26 to be close to the profile attained in the simulations of Kawahara & Kida (2001). The corresponding spanwise and time mean RMS perturbation velocities for the self-sustained state shown in Fig. 27 are also close to values for these quantities simulated under turbulent conditions. The streamwise mean roll/streak structure during a period of streak vacillation with $f = 0$ are shown in Fig. 28 and Fig. 29. In summary this restricted model provides quite accurate simulation of the statistics of this turbulent shear flow.

11. The parametric mechanism maintaining the turbulent state

We wish to gain a clearer understanding of the physical mechanism supporting the turbulent state. In the case of structurally stable equilibrium roll/ streak/ turbulence states oblique waves collocated by the modally stable streak produce Reynolds stress derived torques that support the roll/streak structure. This tendency of the streak to organize oblique wave perturbations producing torques that support the streak is retained in the time-dependent regime and explains the maintenance of the time dependent streamwise mean roll/streak complex by the perturbations. However, the maintenance of the perturbation field in the time dependent regime, which occurs in the absence of forcing (i.e. $f = 0$), remains to be explained. It is tempting to appeal to modal instability of streak snapshots taken in the turbulent regime which imply that instability occurs at least episodically as can be seen from the maximum modal growth rate shown in Fig. 30 for the case with $f = 10$ and in Fig. 31 for $f = 0$. This instability is only notional as the time scale for its growth is nearly the same as the time scale of the state vacillation. Moreover, perturbation growth rate is weakly associated with mode growth rate with correlation of these quantities being 0.2, as can be seen in Fig. 32.

It therefore appears that the eddy variance producing the torque that maintains the roll/streak in the turbulent regime, while arising from shear/perturbation growth processes, is not directly associated with modal instability. In order to verify this an integration of a turbulent state at $R = 800$ for which the instantaneous growth rate is shown in Fig. 33 was performed with the instantaneous flow maintained modally stable by setting the real part of all eigenvalues $\sigma_r + i\sigma_i$ with positive real part to $\sigma_r = -0.001$ at each time step.

The time series before this intervention is shown in Fig. 34 and after the intervention in Fig. 35. Although this intervention introduces a substantial additional dissipation to the system and despite suppression of all modal instability even so turbulence is maintained by non-normal processes because the structure of the eigenmodes has been preserved. In fact the modal stable turbulent state is characterized by a stronger streak which is consistent with suppression of energy extraction from the streak by the inflectional mode.

This experiment shows that in the turbulent state perturbation energy is maintained

by non-normal interaction between the perturbation and the time dependent mean state unrelated to modal instability. This is consistent with optimal growth rates being large in this system and particularly large compared to modal growth rates. There is no lack of growth potential in the optimally growing perturbations but in a time independent flow the associated growth is transient. It is a remarkable fact that in a time dependent mean flow otherwise transient non-normal growth is quite generally sustained to produce asymptotic growth. Perturbation growth in this turbulent regime can be traced to this universal process of destabilization of time dependent systems that is consequent to the necessary non-normality of almost all time-dependent systems (Farrell & Ioannou 1996*b*, 1999; Poulin *et al.* 2003; Pedlosky & Thomson 2003; Farrell & Ioannou 2008*b*; Poulin *et al.* 2010). We conclude that the turbulent state is maintained by a parametric instability that is analogous to the instability of a damped harmonic oscillator with time dependent restoring force, a system which is also non-normal, time dependent and also clearly modally stable at each instant.

However, as in the case of the stable time independent roll/streak equilibria, a mechanism of feedback stabilization is required in addition to a growth process in order to maintain a statistically stable turbulent state. To understand how the parametric instability of the turbulent state is controlled by interaction between the streamwise mean state and the perturbation field to produce bounded statistics consider the equation for perturbation covariance (4.7) with $f = 0$. The mean flow that appears in the dynamical operator A_k is influenced by interaction with the perturbations governed by this operator but if we imagine for heuristic purposes that this mean flow is given, then for $f = 0$ Eq. (4.7) is a linear equation for the evolution of C_k. If we convert C_k to a vector formed by its columns, the covariance evolution dynamics are governed by the time dependent linear operator $\mathcal{A}_k = \mathsf{I} \otimes \mathsf{A}_k + \mathsf{A}_k^* \otimes \mathsf{I}$ where $\otimes$ is the Kronecker product, and $*$ denotes complex conjugation. Asymptotically the covariance will be attracted with exponential accuracy to the structure of the largest Lyapunov exponent associated with $\mathcal{A}_k$. This asymptotic structure is the rank one covariance $\hat{\boldsymbol{\phi}}_k^* \otimes \hat{\boldsymbol{\phi}}_k$ where $\hat{\boldsymbol{\phi}}_k$ is the asymptotic state of the time dependent linear dynamics

$$\frac{\mathrm{d}\hat{\boldsymbol{\phi}}_k}{\mathrm{d}t} = \mathsf{A}_k(\boldsymbol{U}(t))\ \hat{\boldsymbol{\phi}}_k\ , \tag{11.1}$$

with the prescribed $\boldsymbol{U}(t)$. Further, because C_k is bounded, the top Lyapunov exponent associated with this dominant structure $\hat{\boldsymbol{\phi}}_k \otimes \hat{\boldsymbol{\phi}}_k^*$ is exactly $\lambda = 0$. (This Lyapunov exponent should not be confused with the Lyapunov exponent of the full SSST equation in which the mean streamwise velocity is also perturbed. The Lyapunov exponent of the full SSST equations is positive and is obtained from the asymptotic behavior of Eq. (5.2) evaluated about the full time dependent trajectory.) In the case of stable time independent roll/streak equilibria feedback between perturbation and mean flow results in stabilization of the perturbation dynamics but in this case with time dependent dynamics this feedback stabilization instead produces an analogous statistically zero Lyapunov growth rate.

We conclude that perturbation variance is maintained by the universal parametric non-normal mechanism that destabilizes time dependent dynamics and that the otherwise highly unlikely fact that the time dependent perturbation equation (11.1) with mean flow time series $\boldsymbol{U}(t)$ has Lyapunov exponent exactly zero results from the feedback between the perturbation dynamics and the mean flow (4.11) that serves to exactly neutralize the time dependent (11.1) producing a consistent solution trajectory.

12. Minimal representation of shear turbulence dynamics

Asymptotic exponential dominance of the first Lyapunov vector in the parametric time dependent mechanism supporting the turbulent state has important implications for the structure of the perturbation variance in turbulence. Consider first self-sustained turbulence in the SSST system with $f = 0$ in which case the covariance C_k collapses to the rank one covariance $\hat{\phi}_k^* \otimes \hat{\phi}_k$ where $\hat{\phi}_k$ is the first Lyapunov vector of Eq. (11.1). An example of the rapid convergence of an initial high rank perturbation covariance to a single time dependent state is shown in Fig. 36. The same collapse of the covariance occurs when multiple wave numbers are included in the perturbation dynamics because the various C_k do not interact with each other as each advances under the influence of the time dependent A_k and the covariance of the wavenumber k with the largest growth will be asymptotically dominant. An example of state purification with three waves $k/2$, k and $2k$ with $k = 1.143$ is shown in Fig. 37.

This perturbation covariance collapse demonstrates how a minimal self-sustained turbulent state results from the interaction of a single time dependent perturbation structure with the mean flow providing a minimal representation of shear flow turbulence. It also suggests a mechanism by which a dominant coherent structure arises in turbulence and identifies this structure with the top Lyapunov vector of (11.1) together with the associated streamwise mean flow.

13. Laminarization of the turbulent state

Although the turbulent state appears to exist on a chaotic attractor, the laminar flow and the stable roll/streak structures continue to exist for $0 \leqslant f < f_u$ and these eventually attract the state trajectory resulting in laminarization of the turbulent state as is commonly observed to occur in shear turbulence (Brosa 1989; Schmiegel & Eckhardt 1997; Schneider & Eckhardt 2008; Schneider *et al.* 2010). This typically occurs in SSST simulations when the perturbation state becomes transiently configured to couple energy strongly into the streak during their non-normal interaction. With the resulting decrease in perturbation energy the roll is no longer forced sufficiently by perturbation streamwise torque and it decays leaving the streak unsupported so that it too eventually decays leading to laminarization of the state. Examples of the laminarization process at $R = 350$ are shown in Fig. 38.

14. Summary and Conclusion

In this work we have used SSST to study emergence and equilibration of roll/streak structures in forced turbulence and the mechanism maintaining turbulence in a self-sustaining state. The roll/streak structure in forced turbulence is important in its own right but also as a component of a mechanism of bypass transition which typically proceeds from a pre-existing roll/streak structure. We find that this structure grows as an instability of interaction between the forced turbulence and the mean flow and that this instability can equilibrate at finite amplitude to form stable roll/streak structures. The SSST highlights the fundamental role of wave mean flow interaction in the dynamics of turbulence. The SSST instability exploits the optimality of the non-normal roll/streak structure growth mechanism by organizing the ubiquitous torques associated with turbulent Reynolds stress divergence in the cross stream/spanwise plane to force the optimal roll structure. This organization of the Reynolds stress by the streak resulting in forcing of the roll provides the coupling between the streak and roll required to produce insta-

bility from the non-normal lift-up mechanism. This instability effectively transforms the otherwise transient growth of optimal or near optimal perturbations arising in the background turbulence into persistently growing modal structures. We find that at sufficiently high levels of forced turbulence the stable equilibrium roll/streak complex maintained at lower turbulence levels loses structural stability and bifurcates to a time dependent state with realistic turbulent statistics that persists for an extended interval of time even in the absence of forcing and parameterized eddy-eddy nonlinearity ($f = 0$) . Regarding f as a bifurcation parameter, transition to turbulence occurs through a saddle node at $f = f_u$ with stable laminar and roll/streak/turbulence structures existing for $f < f_u$. Once in the turbulent state the system exhibits transient chaos eventually laminarizing for $f < f_u$ to the associated stable laminar or roll/streak state. For $f > f_u$ laminarization does not occur. This persistent turbulent state for $f = 0$ rapidly evolves to a particularly simple minimal representation of turbulence in which the dynamics are limited to the interaction of the streamwise mean flow with a single time dependent streamwise perturbation structure in the sense that the perturbation covariance evolves to have rank one. This transient chaotic state is supported by the universal time dependent parametric destabilization consequent to the necessary non-normality of time dependent dynamics.

This work was supported by NSF ATM-0123389. Discussions with Eli Tziperman and Tobias Schneider are gratefully acknowledged.

Appendix A. Reynolds stress arising from oblique waves in unbounded constant shear flow

Consider the unbounded inviscid constant shear flow $U = \alpha y$. Perturbations in the form:

$$u = \mathrm{Re}\left(\hat{u}(t)\cos(mz)\mathrm{e}^{\mathrm{i}kx+\mathrm{i}l(t)y}\right)\ ,\ v = \mathrm{Re}\left(\hat{v}(t)\cos(mz)\mathrm{e}^{\mathrm{i}kx+\mathrm{i}l(t)y}\right)\ ,\ w = \mathrm{Re}\left(\hat{w}(t)\sin(mz)\mathrm{e}^{\mathrm{i}kx+\mathrm{i}l(t)y}\right)\ . \tag{A 1}$$

evolve according to

$$\frac{\mathrm{d}(K^2(t)\hat{v})}{\mathrm{d}t} = 0\quad ,\quad \frac{\mathrm{d}\hat{\omega}_y}{\mathrm{d}t} = \alpha m\hat{v}\ , \tag{A 2}$$

where $l(t) = l - \alpha k t$, $K^2(t) = k^2 + l^2(t) + m^2$. The cross-stream vorticity amplitude, $\hat{\omega}_y = -m\hat{u} - \mathrm{i}k\hat{w}$, is related to the cross-stream and spanwise velocities by:

$$\hat{w} = -\frac{\mathrm{i}l(t)m}{k^2+m^2}\hat{v} + \frac{\mathrm{i}km}{k^2+m^2}\hat{\omega}_y\ .$$

Solving (A 2) we obtain:

$$\hat{v} = \frac{K^2(0)}{K^2(t)}v_0\ ,\quad \hat{\omega}_y = \omega_{y0} + \frac{mK^4(0)}{k\sqrt{k^2+m^2}K^2(t)}\ \Delta\theta\ v_0\ , \tag{A 3}$$

where subscript 0 denotes the initial value and

$$\Delta\theta = \tan^{-1}\frac{\sqrt{k^2+m^2}}{l(t)} - \tan^{-1}\frac{\sqrt{k^2+m^2}}{l(0)}\ .$$

These solutions in isolation satisfy the nonlinear Navier-Stokes equations (Kelvin 1887; Moffatt 1967; Farrell & Ioannou 1993*a*).

The streamwise mean toque induced by this perturbation field is:

$$\begin{aligned} G_x &= \rho \frac{\partial^2 \overline{vw}}{\partial z^2} \\ &= -\rho m^2 \mathrm{Re}(\hat{v}\hat{w}^*)\ \sin(2mz) \\ &= -\rho \frac{m^2 K^2(0)}{K^2(t)} \mathrm{Re}(v_0 w_0^*)\ \sin(2mz)\ . \end{aligned} \tag{A 4}$$

REFERENCES

Adrian, R. J. 2007 Hairpin vortex organization in wall turbulence. *Physics of Fluids* **19** (4), 041301.

Andersson, P., Berggren, M. & Henningson, D. S. 1999 Optimal disturbances and bypass transition in boundary layers. *Physics of Fluids* **11**, 134–150.

Bakas, N., Ioannou, P. J. & Kefaliakos, G. E. 2001 The emergence of coherent structures in stratified shear flow. *J. Atmos. Sci.* **58**, 2790–2806.

Bamieh, B. & Dahleh, M. 2001 Energy amplification in channel flows with stochastic excitation. *Physics of Fluids* **13**, 3258–3269.

Benney, D. J. 1960 A non-linear theory for oscillations in a parallel flow. *J. Fluid Mech.* **10** (02), 209–236.

Benney, D. J. 1984 The evolution of disturbances in shear flows at high Reynolds numbers. *Stud. Appl. Math.* **70** (02), 1–19.

Berlin, S. & Henningson, D. S. 1999 A nonlinear mechanism for receptivity of free-stream disturbances. *Physics of Fluids* **11** (02), 3749–3760.

Bewley, T. R. & Liu, S. 1998 Optimal and robust control and estimation of linear paths to transition. *J. Fluid Mech.* **365**, 23–57.

Brandt, L. & Henningson, D. S. 2002 Weakly nonlinear analysis of boundary layer receptivity to free-stream disturbances. *Physics of Fluids* **14**, 1426–1441.

Brosa, U. 1989 Turbulence without strange attractor. *J. Stat. Phys.* **55**, 1303–1312.

Brown, G. & Thomas, A. 1977 Large structure in a turbulent boundary layer. *Physics of Fluids* **20**, 243–252.

Brown, R. A. 1970 A secondary flow model for the planetary boundary layer. *J. Atmos. Sci.* **27**, 742–757.

Brown, R. A. 1972 On the inflection point instability of a stratified ekman boundary layer. *J. Atmos. Sci.* **29**, 850–859.

DelSole, T. 1996 Can quasigeostrophic turbulence be modeled stochastically? *J. Atmos. Sci.* **53**, 1617–1633.

DelSole, T. 2001 A simple model for transient eddy momentum fluxes in the upper troposphere. *J. Atmos. Sci.* **58**, 3019–3035.

DelSole, T. 2004 Stochastic models of quasigeostrophic turbulence. *Surveys in Geophysics* **25**, 107–194.

DelSole, T. & Farrell, B. F. 1996 The quasi-linear equilibration of a thermally mantained stochastically excited jet in a quasigeostrophic model. *J. Atmos. Sci.* **53**, 1781–1797.

Drazin, P. G. & Reid, W. H. 1981 *Hydrodynamic Stability*. Cambridge University Press, Cambridge.

Ellingsen, T. & Palm, E. 1975 Stability of linear flow. *Physics of Fluids* **18**, 487–488.

Etling, D. & Brown, R. A. 1993 Roll vortices in the planetary boundary layer: A review. *Bound.-Layer Meteor.* **65**, 215–248.

Farrell, B. F. 1988 Optimal excitation of perturbations in viscous shear flow. *Physics of Fluids* **31**, 2093–2102.

Farrell, B. F. & Ioannou, P. J. 1993*a* Optimal excitation of three dimensional perturbations in viscous constant shear flow. *Physics of Fluids* **5**, 1390–1400.

Farrell, B. F. & Ioannou, P. J. 1993*b* Perturbation growth in shear flow exhibits universality. *Physics of Fluids* **5**, 2298–2300.

Farrell, B. F. & Ioannou, P. J. 1993*c* Stochastic dynamics of baroclinic waves. *J. Atmos. Sci.* **50**, 4044–4057.

Farrell, B. F. & Ioannou, P. J. 1993*d* Stochastic forcing of perturbation variance in unbounded shear and deformation flows. *J. Atmos. Sci.* **50**, 200–211.

Farrell, B. F. & Ioannou, P. J. 1993*e* Stochastic forcing of the linearized Navier-Stokes equations. *Phys. Fluids A* **5**, 2600–2609.

Farrell, B. F. & Ioannou, P. J. 1994 Variance maintained by stochastic forcing of non-normal dynamical systems associated with linearly stable shear flows. *Phys. Rev. Lett.* **72**, 1118–1191.

Farrell, B. F. & Ioannou, P. J. 1995 Stochastic dynamics of the midlatitude atmospheric jet. *J. Atmos. Sci.* **52**, 1642–1656.

Farrell, B. F. & Ioannou, P. J. 1996*a* Generalized stability. Part I: Autonomous operators. *J. Atmos. Sci.* **53**, 2025–2040.

Farrell, B. F. & Ioannou, P. J. 1996*b* Generalized stability. Part II: Non-autonomous operators. *J. Atmos. Sci.* **53**, 2041–2053.

Farrell, B. F. & Ioannou, P. J. 1998*a* Perturbation structure and spectra in turbulent channel flow. *Theor. Comput. Fluid Dyn.* **11**, 215–227.

Farrell, B. F. & Ioannou, P. J. 1998*b* Turbulence supresssion by active control. *Physics of Fluids* **8**, 1257–1268.

Farrell, B. F. & Ioannou, P. J. 1999 Perturbation growth and structure in time dependent flows. *J. Atmos. Sci.* **56**, 3622–3639.

Farrell, B. F. & Ioannou, P. J. 2002 Perturbation growth and structure in uncertain flows. Part II. *J. Atmos. Sci.* **59** (18), 2647–2664.

Farrell, B. F. & Ioannou, P. J. 2003 Structural stability of turbulent jets. *J. Atmos. Sci.* **60**, 2101–2118.

Farrell, B. F. & Ioannou, P. J. 2007 Structure and spacing of jets in barotropic turbulence. *J. Atmos. Sci.* **64**, 3652–3665.

Farrell, B. F. & Ioannou, P. J. 2008*a* Formation of jets by baroclinic turbulence. *J. Atmos. Sci.* **65**, 3353–3375.

Farrell, B. F. & Ioannou, P. J. 2008*b* The stochastic parametric mechanism for generation of surface water waves by wind. *J. Phys. Oceanogr.* **38**, 862–879.

Farrell, B. F. & Ioannou, P. J. 2009 A stochastic structural stability theory model of the drift wave-zonal flow system. *Physics of Plasmas* **16**, 112903.

Foster, R. C 1997 Structure and energetics of optimal Ekman layer perturbations. *J. Fluid Mech.* **333**, 97–123.

Gayme, D. F., McKeon, B. J., Papachristodoulou, A., Bamieh, B. & Doyle, J. C. 2010 A streamwise constant model of turbulence in plane Couette flow. *J. Fluid Mech.* **665**, 99–119.

Gibson, J., Halcrow, J. & Cvitanović, P. 2008 Visualizing the geometry of state space in plane couette flow. *J. Fluid Mech.* **611**, 107–130.

Hall, P. 1990 Taylor-gortler vortices in fully developed or boundary-layer flows: linear theory. *J. Fluid Mech.* **124**, 475–494.

Hall, P. & Sherwin, S. 2010 Streamwise vortices in shear flows: harbingers of transition and the skeleton of coherent structures. *J. Fluid Mech.* **661**, 178–205.

Hall, P. & Smith, F. 1991 On strongly nonlinear vortex/wave interactions in boundary-layer transition. *J. Fluid Mech.* **227**, 641–666.

Hamilton, K., Kim, J. & Waleffe, F. 1995 Regeneration Mechanisms of Near-Wall Turbulence Structures. *J. Fluid Mech.* **287**, 317–348.

Henningson, D. S. 1996 Comment on "Transition in shear flows. Nonlinear normality versus non-normal linearity" [Phys. Fluids 7, 3060 (1995)]. *Physics of Fluids* **8**, 2257–2258.

Henningson, D. S. & Reddy, S. C. 1994 On the role of linear mechanisms in transition to turbulence. *Physics of Fluids* **6**, 1396–1398.

Hill, D. C. 1995 Adjoint systems and their role in the receptivity problem for boundary layers. *J. Fluid Mech.* **292**, 183–204.

Hoepffner, J. & Brandt, L. 2008 Stochastic approach to the receptivity problem applied to bypass transition in boundary layers. *Physics of Fluids* **20**, 024108.

Hogberg, M., Bewley, T. R. & Henningson, D. S. 2003*a* Linear feedback control and estimation of transition in plane channel flow. *J. Fluid Mech.* **481**, 149–175.

Hogberg, M., Bewley, T. R. & Henningson, D. S. 2003*b* Relaminarization of Re=1000 turbulence using linear state-feedback control. *Physics of Fluids* **15**, 3572–3575.

Hutchins, N. & Marusic, I. 2007 Evidence of very long meandering features in the logarithmic region of turbulent boundary layers. *J. Fluid Mech.* **579**, 1–28.

Hwang, Y. & Cossu, C. 2010*a* Amplification of coherent structures in the turbulent Couette flow: an input-output analysis at low Reynolds number. *J. Fluid Mech.* **643**, 333–348.

Hwang, Y. & Cossu, C. 2010*b* Linear non-normal energy amplification of harmonic and stochastic forcing in the turbulent channel flow. *J. Fluid Mech.* **664**, 51–73.

Jang, P. S., Benney, D. J. & Gran, R. L. 1986 On the origin of streamwise vortices in a turbulent boundary layer. *J. Fluid Mech.* **169**, 109–123.

Jimenez, J. & Moin, P. 1991 The minimal flow unit in near wall turbulence. *J. Fluid Mech.* **225**, 213–240.

Jimenez, J & Pinelli, A 1999 The autonomous cycle of near-wall turbulence. *J. Fluid Mech.* **389**, 335–359.

Jovanovic, M. & Bamieh, B. 2005 Componentwise energy amplification in channel flows. *J. Fluid Mech.* **534**, 145–183.

Kawahara, G. & Kida, S. 2001 Periodic motion embedded in plane Couette turbulence: regeneration cycle and burst. *J. Fluid Mech.* **449**, 291–300.

Kelvin, Lord 1887 Stability of fluid motion: rectilinear motion of viscous fluid between two parallel planes. *Phil. Mag. (5)* **24**, 188–196.

Kim, J. & Bewley, T. R. 2007 A linear systems approach to flow control. *Annu. Rev. Fluid Mech.* **39**, 383–417.

Kim, J. & Lim, J. 2000 A linear process in wall bounded turbulent shear flows. *Physics of Fluids* **12**, 1885–1888.

Kim, J., Moin, P. & Moser, R. 1987 Turbulence statistics in fully developed channel flow at low Reynolds number. *J. Fluid Mech.* **177**, 133–166.

Klebanoff, P. S., Tidstrom, K. D. & Sargent, L. M. 1962 The three-dimensional nature of boundary-layer instability. *J. Fluid Mech.* **12**, 1–34.

Kline, S. J., Reynolds, W. C., Schraub, F. A & Runstadler, P. W. 1967 The structure of turbulent boundary layers. *J. Fluid Mech.* **30**, 741–773.

Komminaho, J., Lundbladh, A. & Johansson, A. 1996 Very large structures in plane turbulent Couette flow. *J. Fluid Mech.* **320**, 259–285.

Kuo, H. 1963 Perturbations of plane Couette flow in a stratified fluid and origin of cloud streets. *Physics of Fluids* **6**, 145–211.

Landahl, M. T. 1980 A note on an algebraic instability of inviscid parallel shear flows. *J. Fluid Mech.* **98**, 243.

Laval, J.-P., Dubrulle, B. & McWilliams, J. C. 2003 Langevin models of turbulence: Renormalization group, distant interaction algorithms or rapid distortion theory? *Physics of Fluids* **15**, 1327–1339.

LeMone, M. A. 1973 The structure and dynamics of horizontal roll vortices in the planetary boundary layer. *J. Atmos. Sci.* **30**, 1077–1091.

LeMone, M. A. 1976 Modulation of turbulence energy by longitudinal rolls in an unstable planetary boundary layer. *J. Atmos. Sci.* **33**, 1308–1320.

Lin, C-L., McWilliams, J. C., Moeng, C-H. & Sulivan, P. 1996 Coherent structures and dynamics in a neutrally stratified planetary boundary layer flow. *Physics of Fluids* **8**, 2626–2639.

Luchini, P. 2000 Reynolds-number-independent instability of the boundary layer over a flat surface: optimal perturbations. *J. Fluid Mech.* **404**, 289–309.

Matsubara, M. & Alfredsson, P. H. 2001 Disturbance growth in boundary layers subjected to free-stream turbulence. *J. Fluid Mech.* **430**, 149–168.

Moeng, C-H. & Sulivan, P. 1994 A comparison of shear and buoyancy driven planetary boundary layer flows. *J. Atmos. Sci.* **51**, 9991022.

Moffatt, K. 1967 The interaction of turbulence with strong wind shear. In *Atmospheric Turbulence and Radio Wave Propagation* (ed. A. M. Yaglom & V. I. Tatarskii). Nauka, Moscow.

Pedlosky, J. & Thomson, J. 2003 Baroclinic instability of time-dependent currents. *J. Fluid Mech.* **490**, 189–215.

Phillips, W. R. C., Wu, Z. & Lumley, J. L. 1996 On the formation of longitudinal vortices in a turbulent boundary layer over wavy terrain. *J. Fluid Mech.* **326**, 321–341.

Poulin, F. J., Flierl, G. R. & Pedlosky, J. 2003 Parametric instability in oscillatory shear flows. *J. Fluid Mech.* **481**, 329–353.

Poulin, Francis J., Flierl, Glenn R. & Pedlosky, Joseph 2010 The baroclinic adjustment of time-dependent shear flows. *Journal of Physical Oceanography* **40**, 1851–1865.

Reddy, S. C., Schmid, P. J., Baggett, J. S. & Henningson, D. S. 1998 On the stability of streamwise streaks and transition thresholds in plane channel flows. *J. Fluid Mech.* **365**, 269–303.

Schmid, P. J. & Henningson, D. S. 1992 A new mechanism for rapid transition involving a pair of oblique waves. *Physics of Fluids A: Fluid Dynamics* **4**, 1986–1989.

Schmid, P. J. & Henningson, D. S. 2001 *Stability and Transition in Shear Flows*. Springer, New York.

Schmiegel, Armin & Eckhardt, Bruno 1997 Fractal stability border in plane couette flow. *Phys. Rev. Lett.* **79** (26), 5250–5253.

Schneider, Tobias M., De Lillo, Filippo, Buehrle, Juergen, Eckhardt, Bruno, Dörnemann, Tim, Dörnemann, Kay & Freisleben, Bernd 2010 Transient turbulence in plane couette flow. *Phys. Rev. E* **81**, 015301.

Schneider, Tobias M. & Eckhardt, Bruno 2008 Lifetime statistics in transitional pipe flow. *Phys. Rev. E* **78** (4), 046310.

Schoppa, W. & Hussain, F. 2000 Coherent structure dynamics in near-wall turbulence. *Fluid Dynamics Research* **26**, 119–139.

Schoppa, W. & Hussain, F. 2002 Coherent structure generation in near-wall turbulence. *J. Fluid Mech.* **453**, 57–108.

Smith, C. R. & Metzler, S. P. 1983 The characteristics of low-speed streaks in the near-wall region of a turbulent boundary layer. *J. Fluid Mech.* **129**, 27–54.

Townsend, A. A. 1956 *The Structure of Turbulent Shear Flow*. Cambridge University Press, Cambridge.

Waleffe, F. 1997 On a self-sustaining process in shear flows. *Phys. Fluids A* **9**, 883–900.

Waleffe, F. 2003 Homotopy of exact coherent structures in plane shear flows. *Physics of Fluids* **15**, 1517–1534.

Westin, K. J. A., Boiko, A. V., Klingmann, B. G. B., Kozlov, V. V. & Alfredsson, P. H. 1994 Experiments in a boundary layer subjected to free stream turbulence. Part 1. Boundary layer structure and receptivity. *J. Fluid Mech.* **281**, 193–218.

Whitaker, J. S. & Sardeshmukh, P. D. 1998 A linear theory of extratropical synoptic eddy statistics. *J. Atmos. Sci.* **55**, 237–258.

Wu, X. & Moin, P. 2009 Direct numerical simulation of turbulence in a nominally zero-pressure-gradient flat-plate boundary layer. *J. Fluid Mech.* **630**, 5–41.

Zhang, Y. & Held, I. M. 1999 A linear stochastic model of a GCM's midlatitude storm tracks. *J. Atmos. Sci.* **56**, 3416–3435.

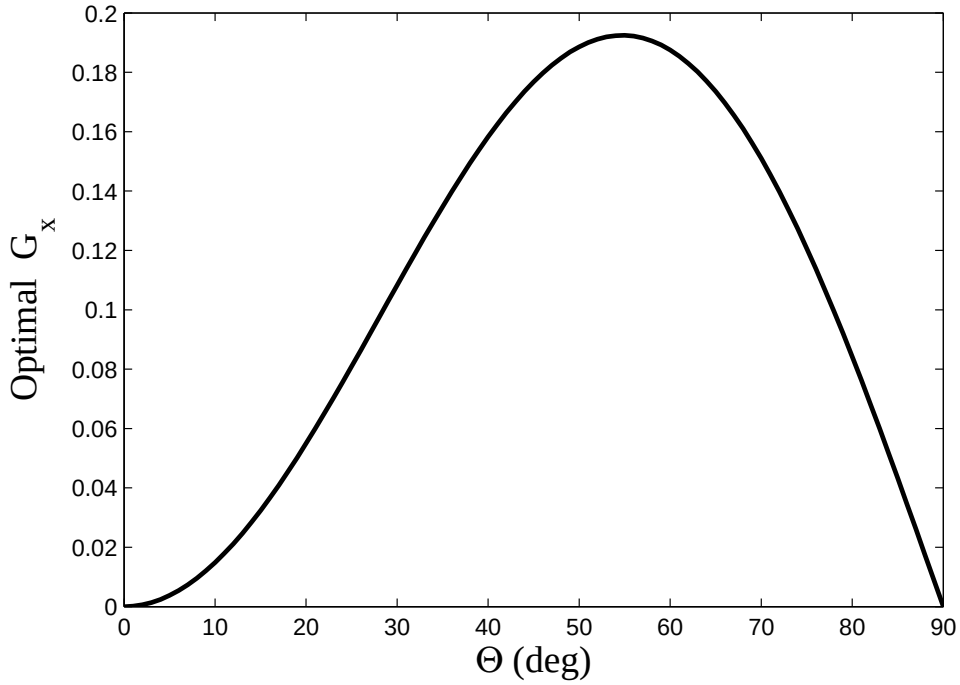

FIGURE 1. The optimal mean streamwise torque produced by oblique waves of the form (2.3). The maximum occurs at angle of obliquity $\Theta = 54.7$. The optimal torque does not depend on the optimizing time. Angle of obliquity $\Theta = 90$ corresponds to perturbations that do not vary in the streamwise direction; $\Theta = 0$ to perturbations that do not vary in the spanwise direction.

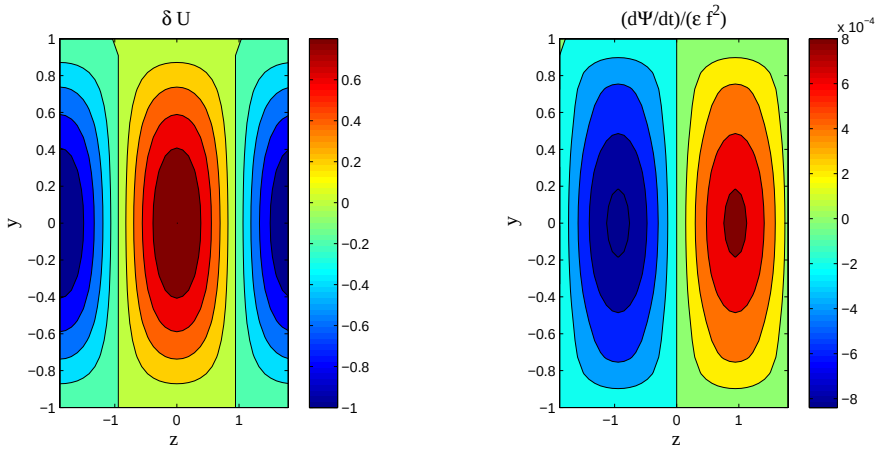

FIGURE 2. Left: Streak perturbation $\delta U = \epsilon \cos(\pi y/(2L_y)) \cos(2\pi z/L_z)$ imposed on a background Couette flow to examine the mechanism of turbulent Reynolds stress organization. Right: Resulting equilibrium Reynolds stress divergence induced tendency in the cross-stream/spanwise streamfunction, $d\Psi/dt$, normalized by the mean flow perturbation amplitude, ϵ, and the square of the forcing amplitude parameter, f, in the limit $\epsilon \to 0$. Imposition of a spanwise perturbation breaks the spanwise symmetry of the Couette flow producing a coherent streamwise torque proportional to both the mean flow perturbation and the eddy variance. The channel dimensions are $L_y = 1$, $L_z = 1.2\pi$, the Reynolds number is $R = 400$, and $k = 2\pi/(1.75\pi)$.

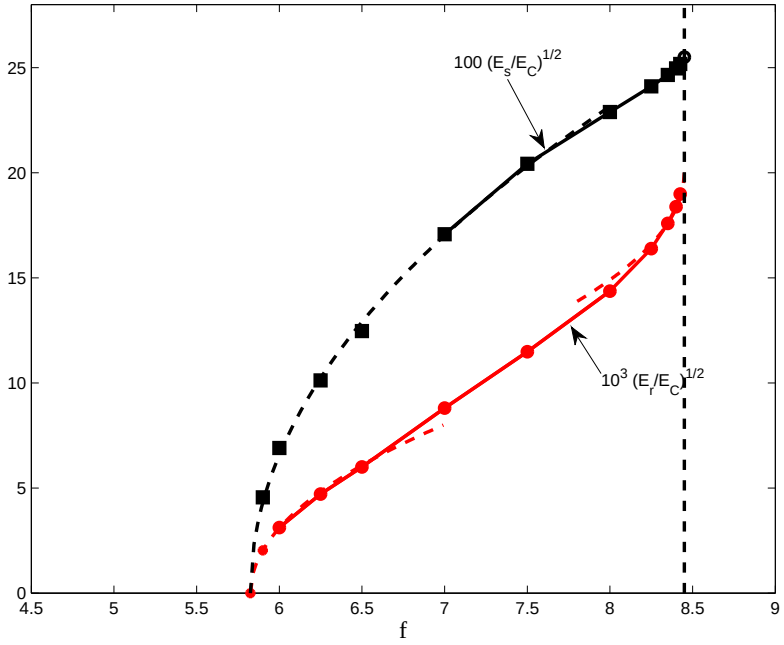

FIGURE 3. Bifurcation diagram of the roll/streak structure as a function of f. At $f_c = 5.825$ the spanwise uniform equilibrium bifurcates to a spanwise dependent roll/streak equilibrium. Shown are normalized streak strength, $100(E_s/E_C)^{1/2}$ (squares) and normalized roll strength, $10^3(E_r/E_C)^{1/2}$ (circles). The dashed line indicates the $\sqrt{f - f_c}$ dependence of the roll and streak amplitude as the critical f_c is approached. The stable equilibria extend up to $f_u = 8.45$; at which point the perturbation stable roll/streak equilibrium becomes structurally unstable. The dashed line indicates the $\sqrt{f_u - f}$ dependence of the roll and streak amplitude as the critical f_u is approached. Parameters correspond to the channel: length $L_x = 1.75\pi$, spanwise width $L_z = 1.2\pi$, half cross-stream height $L_y = 1.0$ and $R = 400$. The perturbation streamwise wavenumber, $k = 1.143$, corresponds to the gravest mode in the channel.

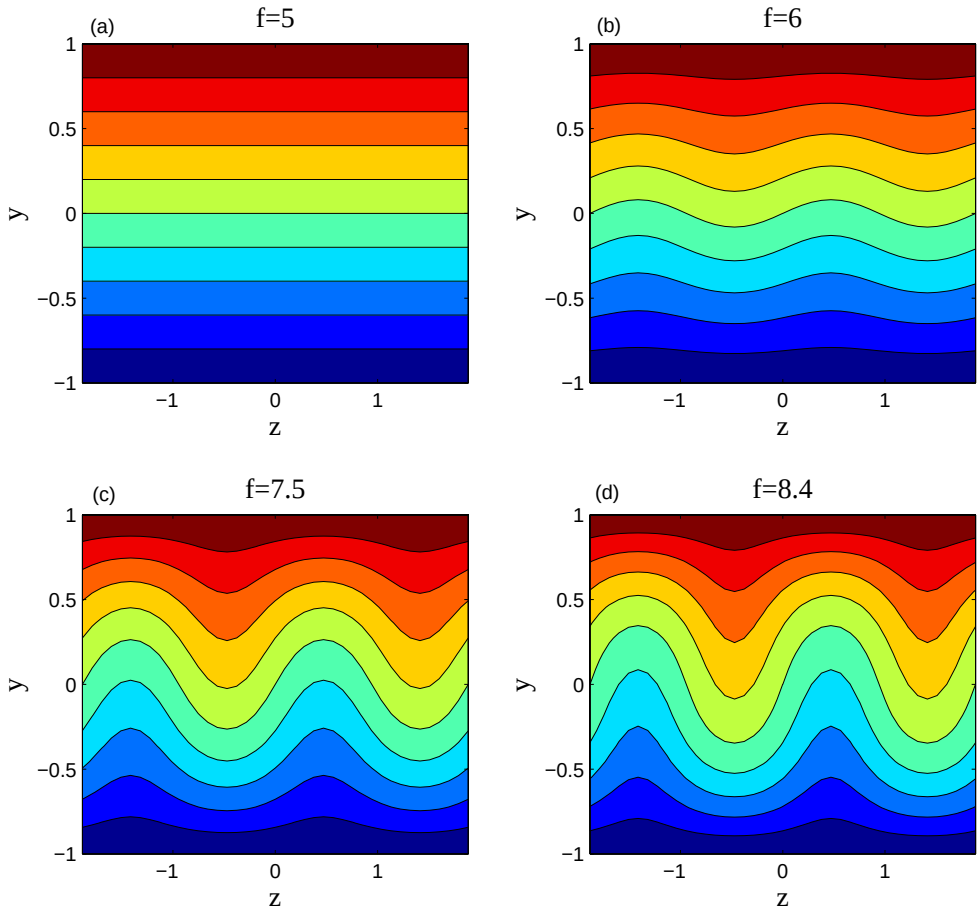

FIGURE 4. Streamwise mean velocity for the SSST equilibria at various values of f. (a): At $f = 5$ the equilibrium is spanwise uniform. (b): At $f = 6$ the spanwise independent flow is structurally unstable and the associated equilibrium has a weak streak. (c): The equilibrium at $f = 7.5$. (d): The equilibrium at $f = 8.4$. All equilibria are perturbation stable. Parameters are as in Fig. 3.

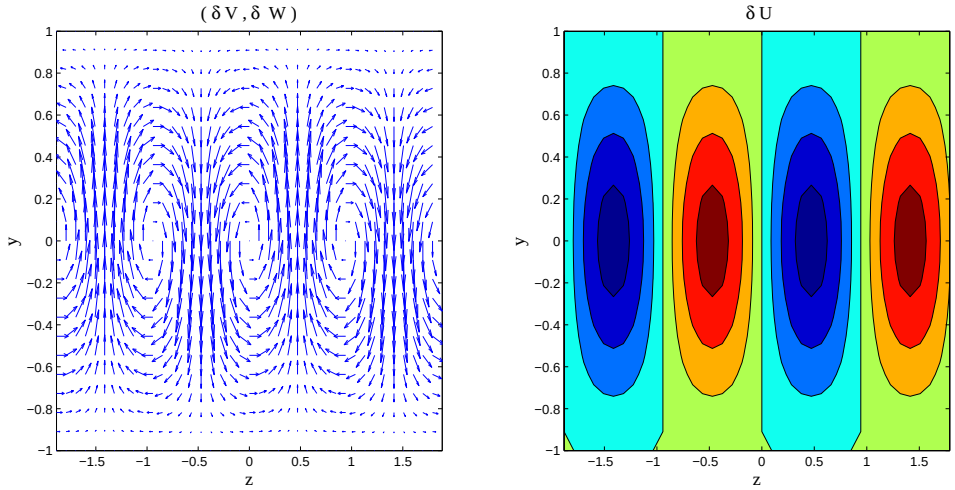

FIGURE 5. The most unstable eigenfunction of the SSST system linearized about the structurally unstable equilibrium with no spanwise variation at $f = 8.4$. The growth rate of this mode is $\lambda = 0.014$. Left: streamwise mean cross-stream/spanwise velocity vectors $(\delta V, \delta W)$ in the cross-stream/spanwise plane. Right: streamwise mean streamwise velocity δU. The ratio of the maxima of the fields $(\delta U, \delta V, \delta W)$ is $(1, 0.06, 0.03)$. Parameters are as in Fig. 3.

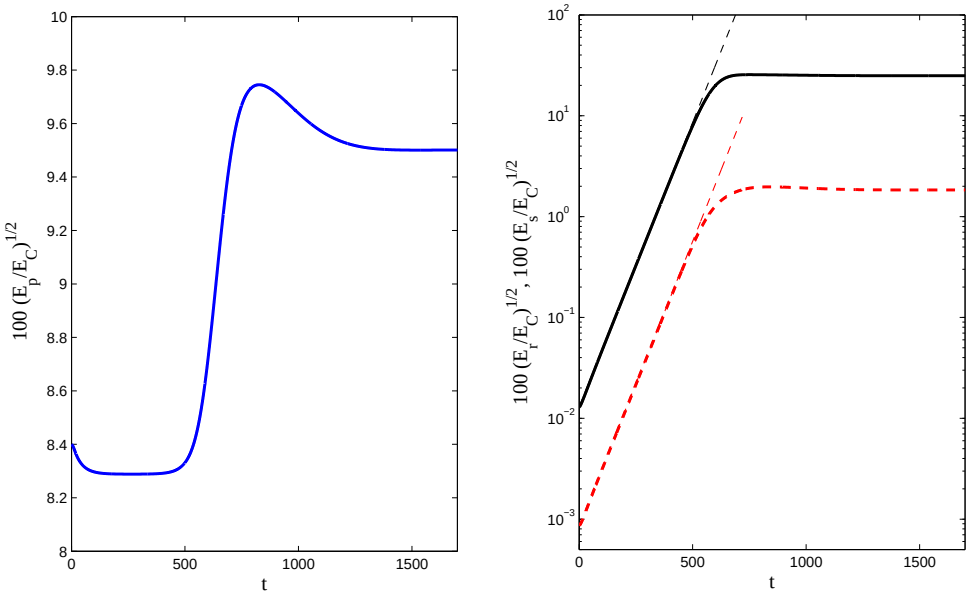

FIGURE 6. Left: Evolution of normalized eddy kinetic energy $100\sqrt{E_p/E_C}$ after the structurally unstable spanwise independent equilibrium is perturbed by the most unstable streak perturbation shown in Fig. 5. The flow equilibrates to the roll/streak equilibrium shown in Fig. 4d. Right: Growth of the streak energy $100\sqrt{E_s/E_C}$ and roll energy $100\sqrt{E_r/E_C}$ is initially exponential with growth rate $\lambda = 0.014$. Parameters are as in Fig. 3 and $f = 8.4$.

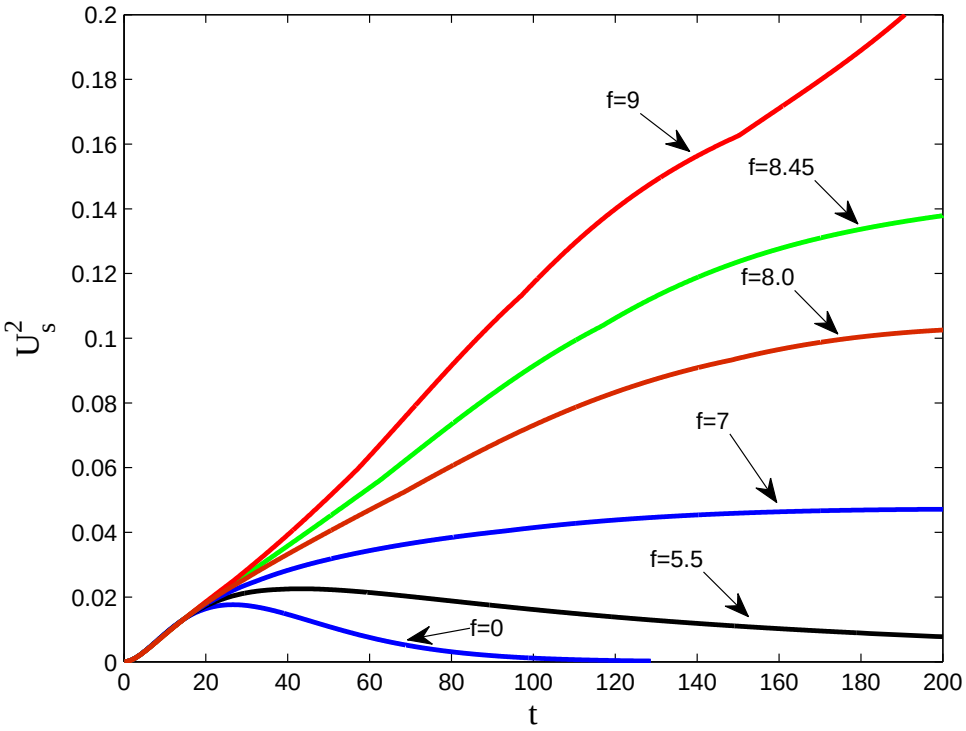

FIGURE 7. Evolution of the maximum streak velocity U_s^2 under the forcing amplitudes $f = 0,\ 5.5,\ 6,\ 7,\ 8,\ 8.45,\ 9$. The initial condition consists of the streamwise independent optimal perturbation for t=50 and spanwise wavenumber $l = 4\pi/L_z$. The amplitude of the initial perturbation streak velocity is taken to be 0.06% of the maximum velocity of the Couette flow in the channel. Note that for $f < f_c = 5.82$ the streak initially grows but then decays, with the rate of decay reduced by the eddy forcing. For $f_c < f < f_u = 8.45$ the optimal evolves to a non-decaying roll/streak equilibrium structure, while for $f > f_u$ the roll/streak becomes structurally unstable and eventually time dependent (not shown). Parameters are as in Fig. 3.

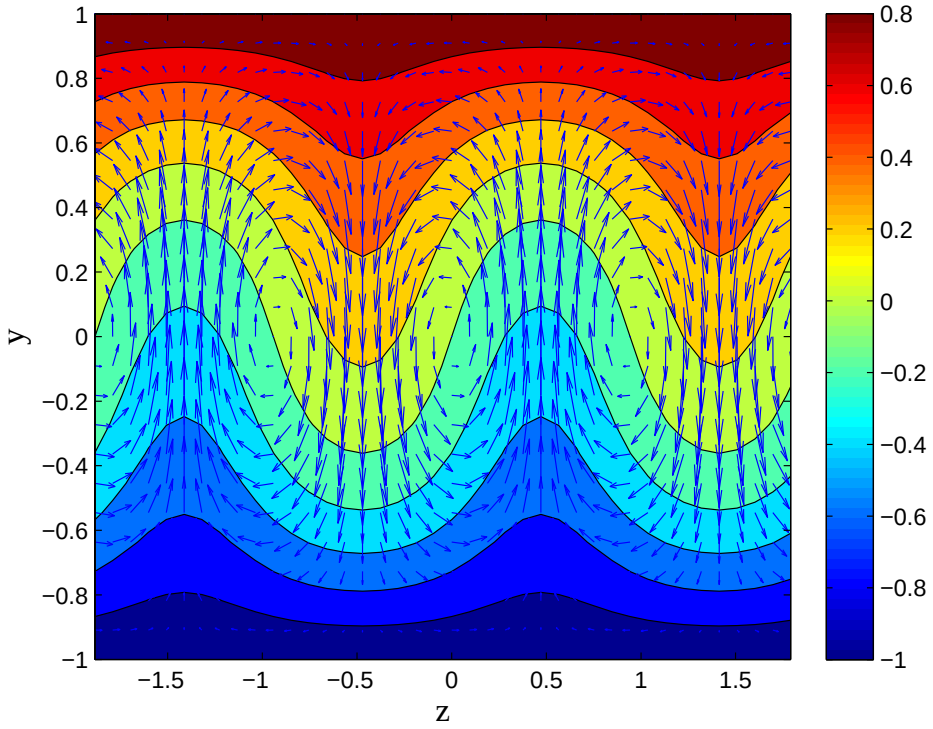

FIGURE 8. Streamwise mean streamwise flow $U(y,z)$ (contours) and roll vector velocities (V,W) for the laminar roll-streak equilibrium at $f = 8.4$ just before the structural instability. The maximum streak velocity U_s is 0.26, the maximum V is 0.02 and the maximum W is 0.009. Parameters are as in Fig. 3.

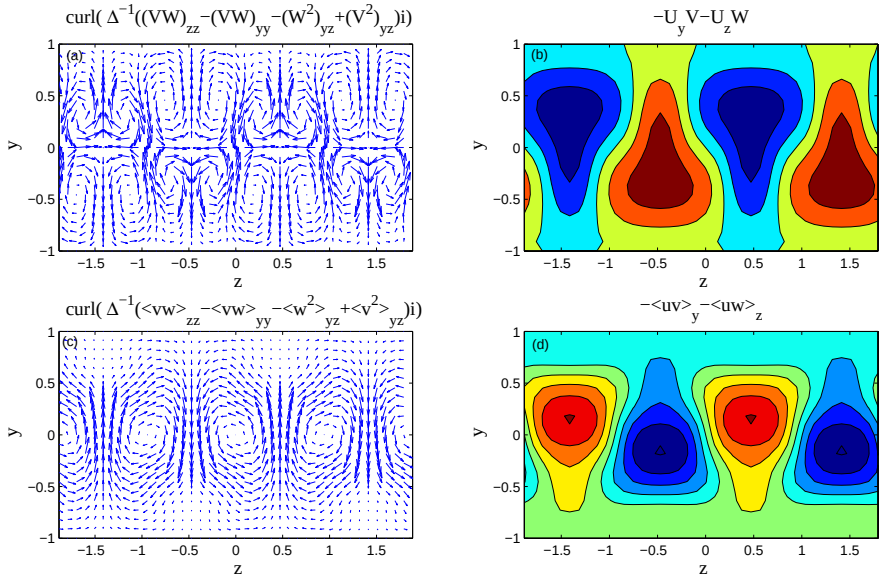

FIGURE 9. For the equilibrium shown in Fig. 8; (a): acceleration vectors, $(\dot{V}, \dot{W})$, of the streamwise mean roll circulation induced by the mean velocity field, the maximum $\dot{V}$ is 10^{-4}. (b): acceleration of the mean streamwise flow, $\dot{U}$, induced by the streamwise mean roll circulation, the maximum $\dot{U}$ is 10^{-2}, mainly due to the lift-up mechanism. (c): acceleration vectors, $(\dot{V}, \dot{W})$, of the streamwise mean roll circulation induced by the eddy field, the maximum $\dot{V}$ is 10^{-3}. (d): acceleration of the mean streamwise flow, $\dot{U}$, induced by the eddy field, the maximum $\dot{U}$ is 10^{-2}. The streaks are maintained by the lift-up mechanism while the direct effect of the eddy field is to decelerate the streaks.

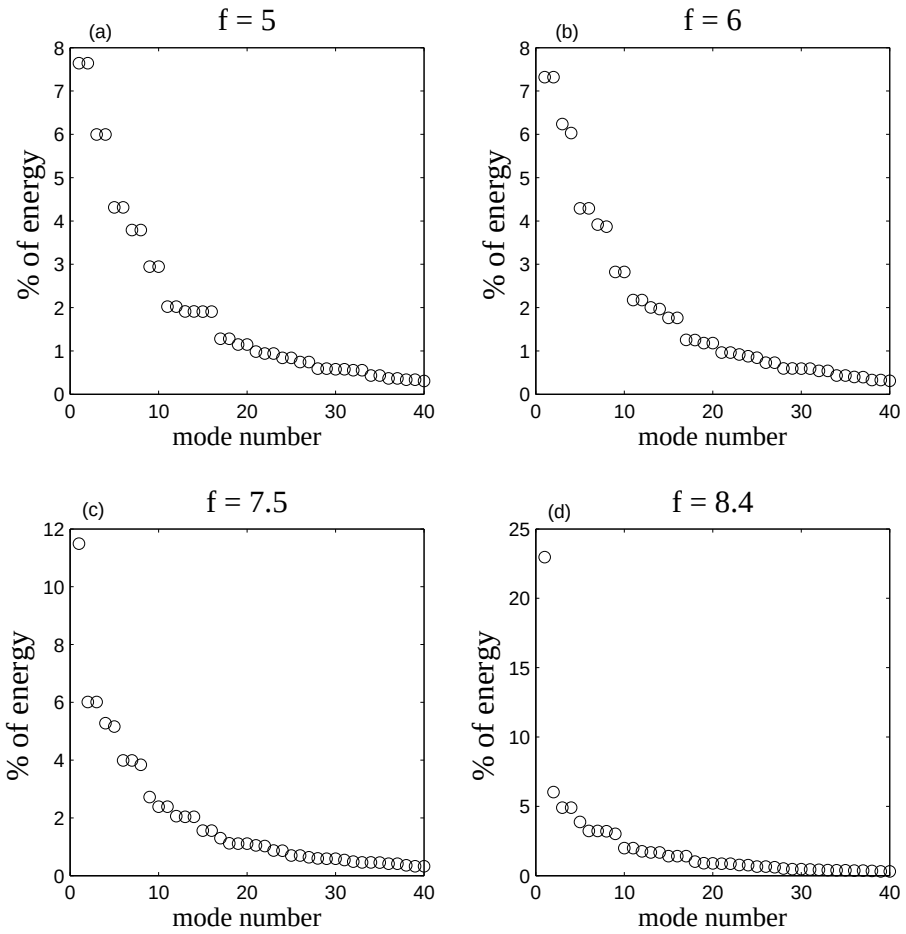

FIGURE 10. Percentage contribution of the leading EOF's of the equilibrium covariance to the total eddy mean energy maintained by the equilibria shown in Fig. 4.

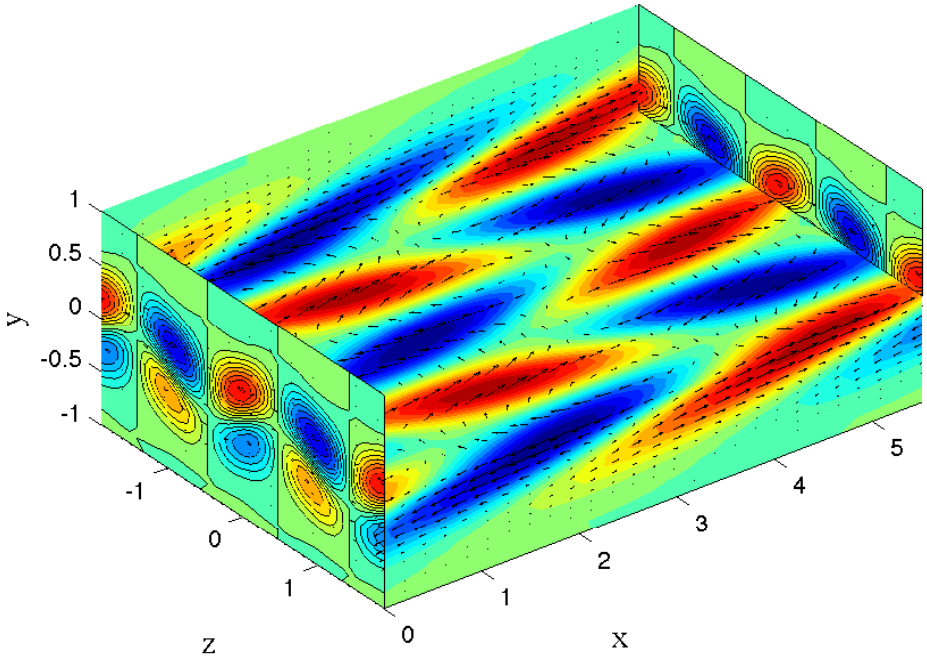

FIGURE 11. Velocity field of the gravest EOF accounting for 24% of the eddy energy for the equilibrium with $f = 8.4$ shown in Fig. 8. Velocity vectors are superposed on contours of streamwise velocity.

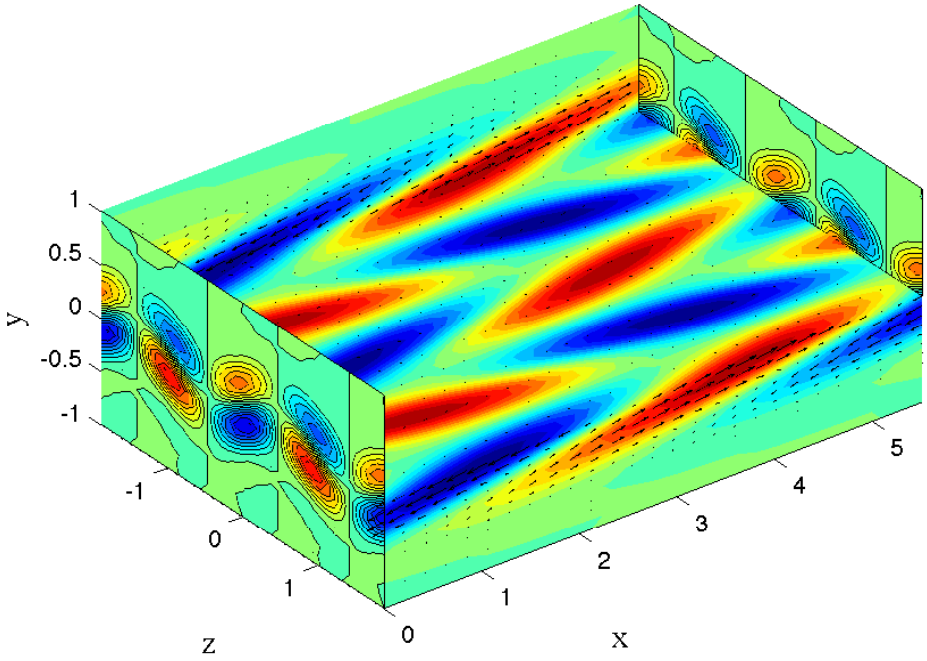

FIGURE 12. Velocity field of the least stable mode of the streamwise flow at the equilibrium with $f = 8.4$ shown in Fig. 8.

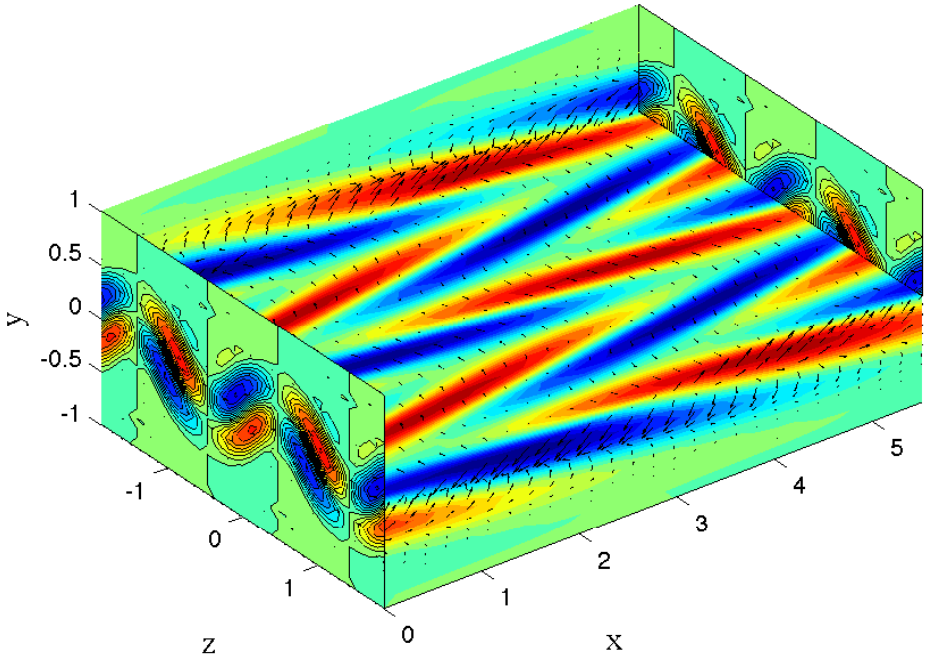

FIGURE 13. Velocity field of the adjoint in the energy inner product of the least stable mode for the equilibrium at $f = 8.4$ shown in Fig. 8. The adjoint is the optimal excitation of the mode and an initial condition consisting of the adjoint with unit energy excites the least stable mode a factor of 1900 greater than an initial condition consisting of the least stable mode itself with unit energy demonstrating that the mode amplitude derives almost entirely from non-normal growth processes.

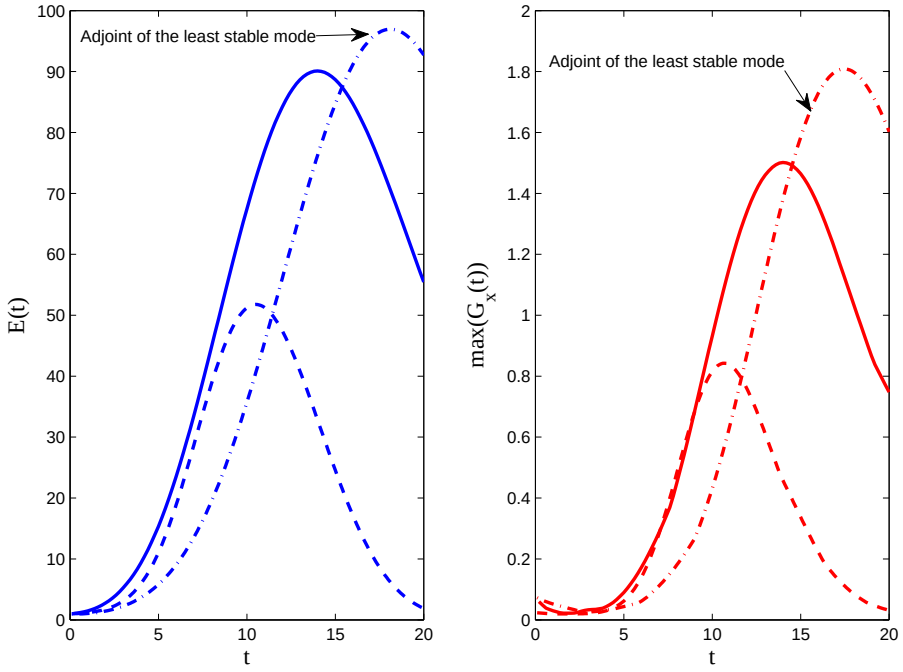

FIGURE 14. Left : Energy of the optimal perturbation that maximizes energy growth at $t = 10$ as a function of time for the equilibrium flow with $f = 8.4$ (solid) for which there is an equilibrium roll/streak and $f = 5$ (dashed) for which there is no streak. Also shown is the energy growth associated with a unit energy initial condition consisting of the adjoint in the energy metric of the least damped mode for the equilibrium with $f = 8.4$ (dash-dot). Right: Time development of the maximum mean streamwise torque induced by the Reynold's stresses of the corresponding evolving optimals and adjoint. This figure demonstrates that both the mode amplitude and its contribution to the streamwise mean torque are due to non-normal growth processes and that obliques waves, which are the short term optimal perturbation, produce through their Reynolds stress streamwise mean torques that maintain the roll circulation regardless of the presence of the streak. All modes in these flows are exponentially stable.

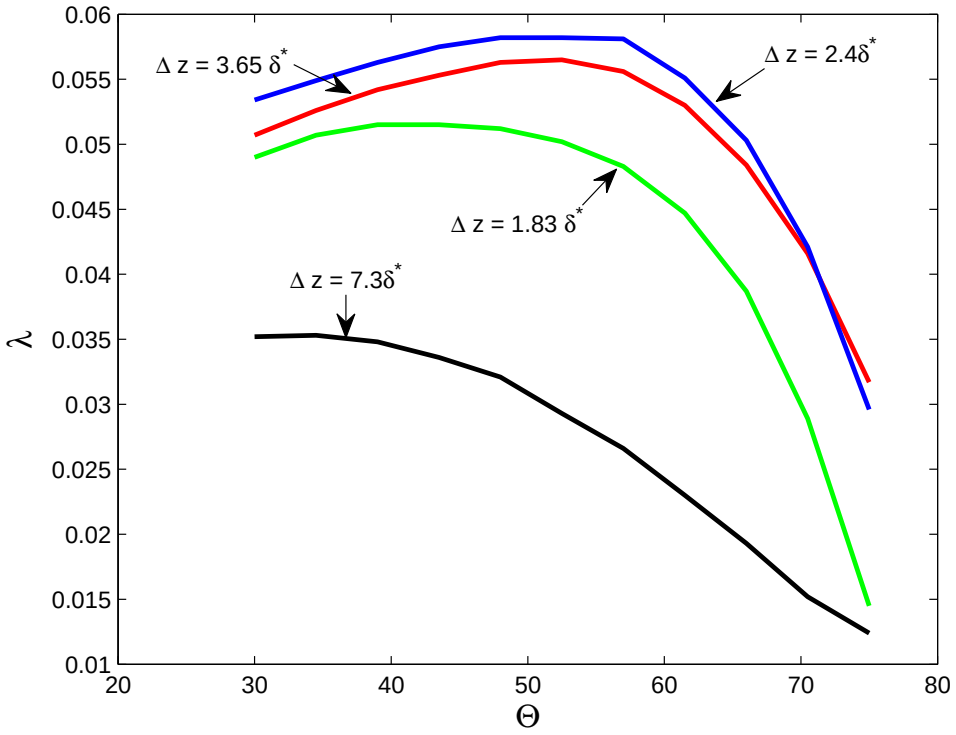

FIGURE 15. Growth rate, λ, of the structurally unstable streaks in a Blasius boundary layer as a function of perturbation obliquity $\Theta \equiv \tan^{-1}(m/k)$ and streak spacing Δz, at Reynolds number based on displacement thickness $R_{\delta^*} = 690$. Maximum growth rate occurs for streak spanwise wavenumber 3 which corresponds to streak spacing $\Delta z = 2.4\delta^*$ or $50y^+$ wall units. Also shown are the growth rates for streak spacing with wavenumner $1, 2, 4$. The channel width is $L_z = 4\pi$, the noise level corresponds to maximum RMS streamwise fluctuations that are 1% of the mean flow and $L_y = 7$.

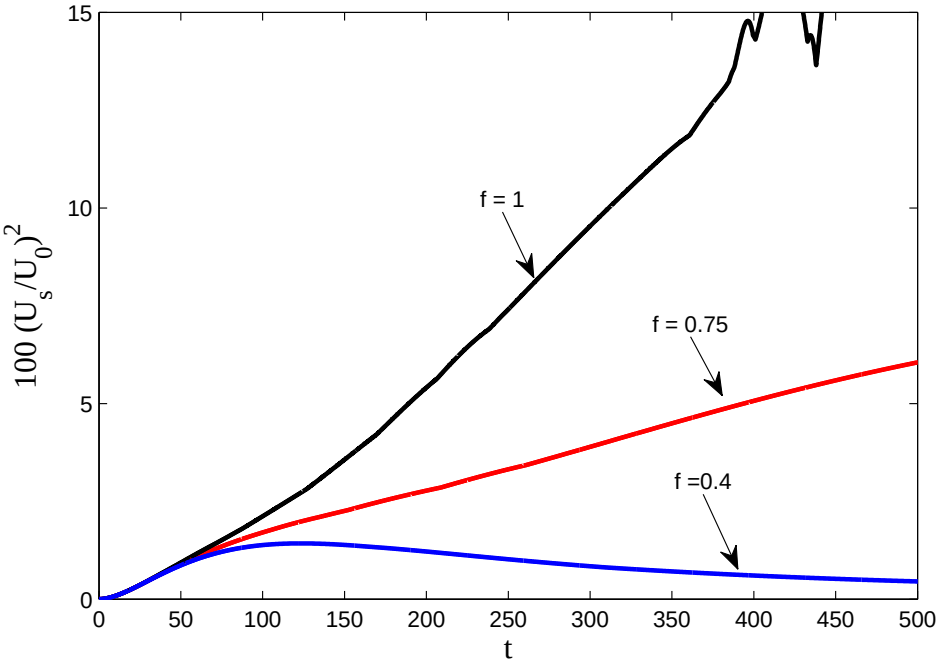

FIGURE 16. Evolution of the maximum streak velocity U_s^2 for perturbation forcing $f = 0.4,\ 0.75,\ 1$ at $k = 1$ and $R_{\delta*} = 600$. The initial condition consists of the streamwise independent perturbation with spanwise wavenumber $m = 1.5$ that optimizes energy growth at $t = 40$. Note that for $f < 0.475$ the streak initially grows but then decays, with the rate of decay reduced by the eddy forcing. For $f > 0.475$ the roll/streak grows and eventually becomes time dependent.

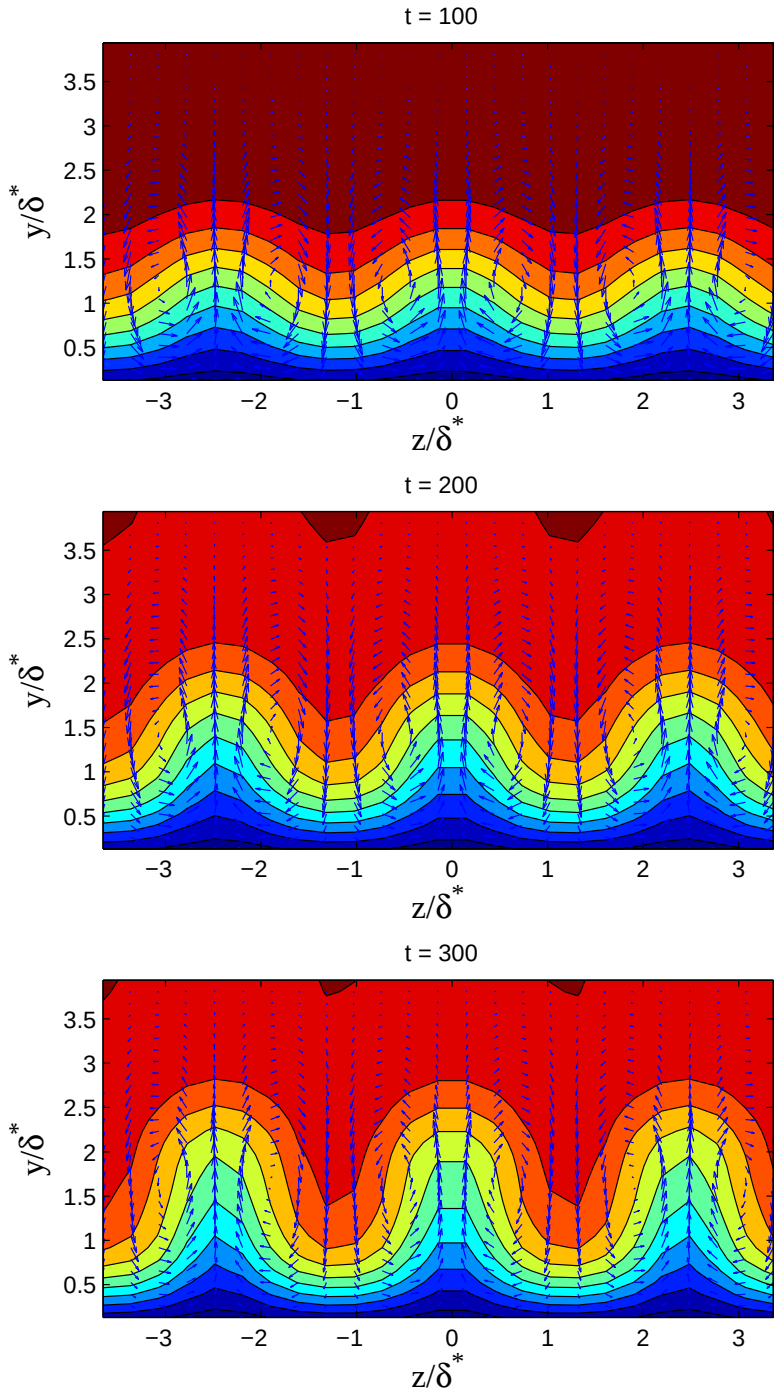

FIGURE 17. Streamwise mean streamwise flow $U(y,z)$ (contours) and roll vector velocities (V,W) at $t = 100,\ 200,\ 300$ before breakdown for the evolving roll/streak shown in Fig. 16 for forcing $f = 1$.

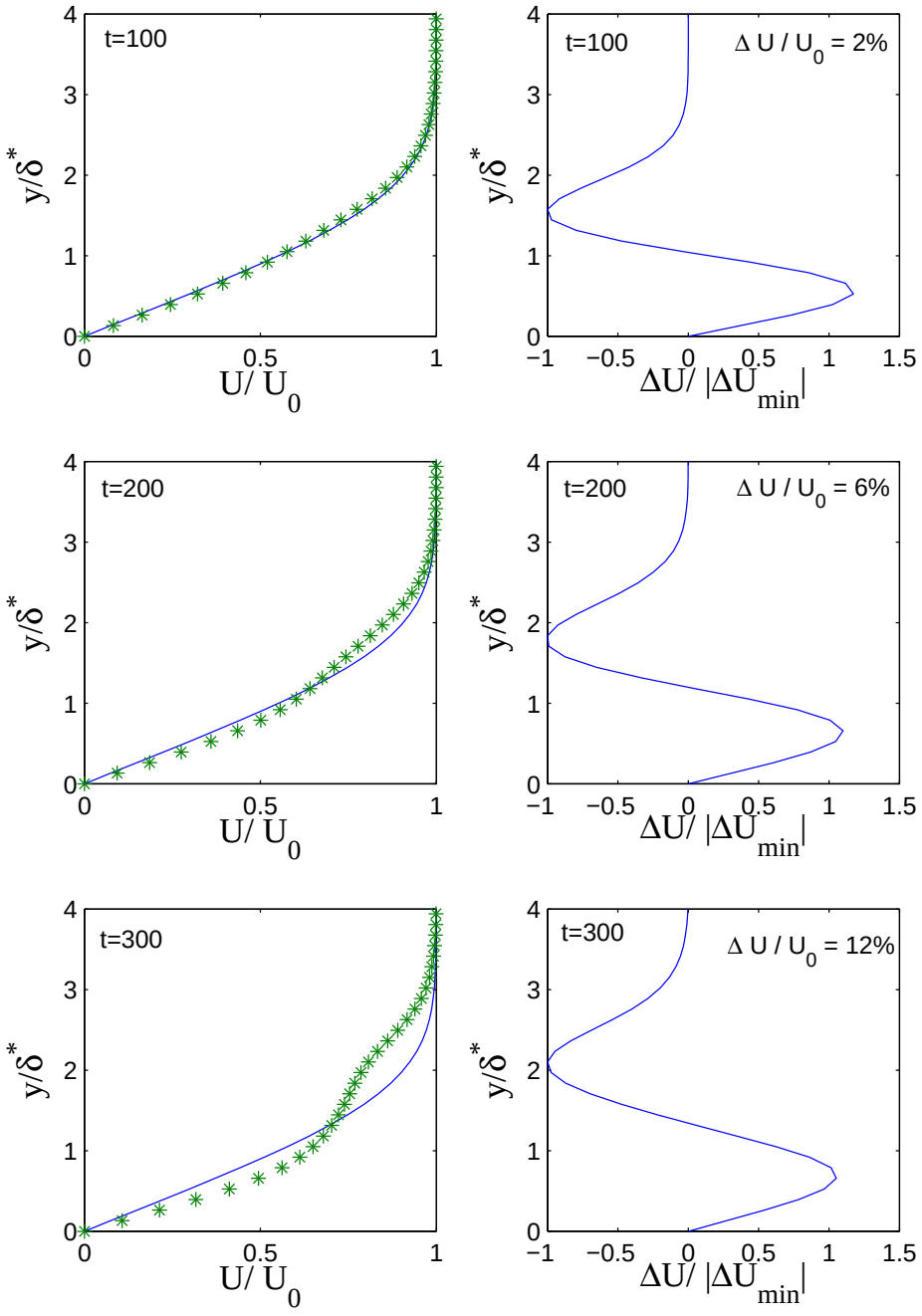

FIGURE 18. Left: The instantaneous spanwise averaged $[U]$ velocity (marked with stars) at times $t = 100,\ 200,\ 300$ and the laminar Blasius velocity profile. The corresponding structure of the streamwise flow is shown in Fig. 17. Right: the instantaneous velocity difference between the instantaneous $[U]$ and the Blasius profile, normalized by the minimum value of this defect. The amplitude of the defect at $t = 100$ is 2% of the velocity U_0 at the top of the boundary layer. It becomes only 6% by $t = 200$ although the streak is highly inflected in the spanwise direction. The shape of the normalized velocity defect changes little during transition.

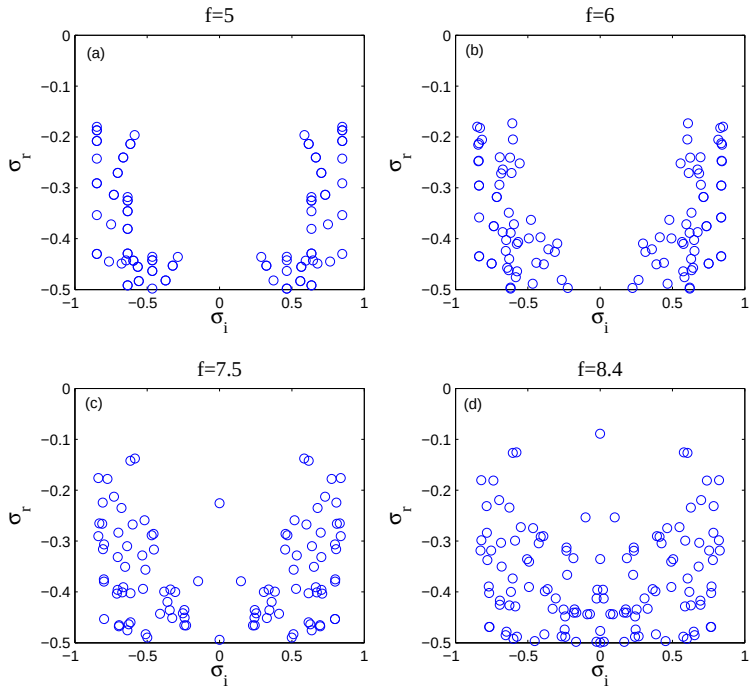

FIGURE 19. The least stable eigenvalues (σ_r, σ_i) of the operators A_k that govern the perturbation stability of the equilibrium flows shown in Fig. 4. All the flows are perturbation stable. Note the emergence of a mode with $\sigma_i = 0$ as the streak increases in magnitude. Parameters are as in Fig. 3.

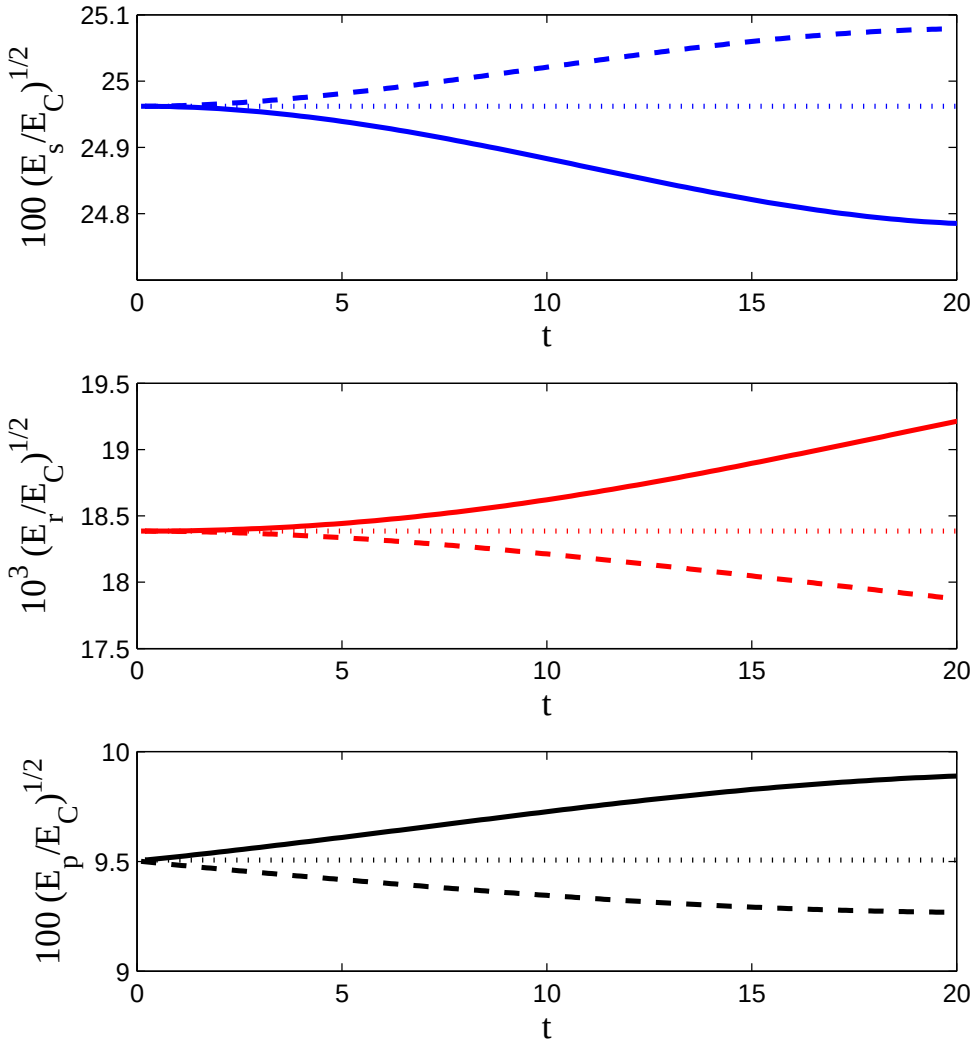

FIGURE 20. Streak amplitude $100\sqrt{E_s/E_C}$ (top panel), roll amplitude $10^3\sqrt{E_r/E_C}$ (middle panel), and RMS perturbation velocity amplitude $100\sqrt{E_p/E_C}$ (bottom panel) as a function of time for decrease (solid) and increase (dashed) in the damping rate of the inflectional mode compared to its damping rate at equilibrium. The corresponding energies at equilibrium are also shown (dotted). The equilibrium is that at $f = 8.4$ shown in Fig. 8. The inflectional mode clearly damps rather than drives the streak.

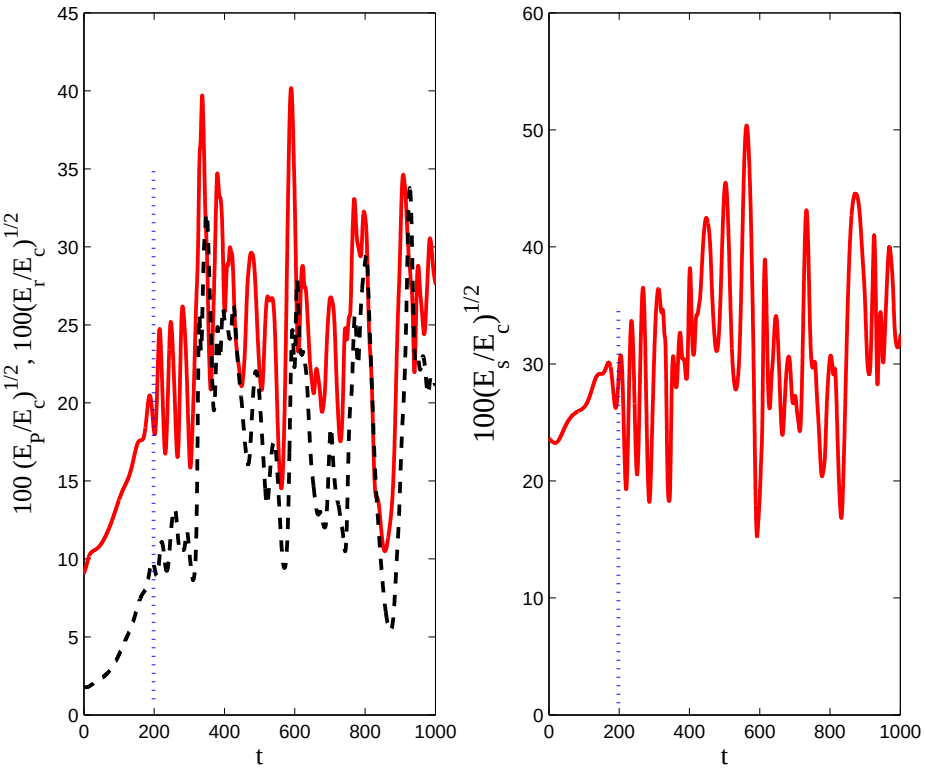

FIGURE 21. Left: Evolution of eddy kinetic energy, $100\sqrt{E_p/E_C}$ and roll energy, $100\sqrt{E_r/E_C}$ (dashed), for $f = 10$. Right: Evolution of the streak energy, $100\sqrt{E_s/E_C}$. For this excitation parameter the roll-streak equilibria are structurally unstable and the flow transitions to a turbulent state. The initial state is the laminar roll-streak equilibrium for STM parameter $f = 8.4$ shown in Fig. 8. The dotted line at $t = 200$ marks the time when the instantaneous streamwise mean flow becomes perturbation unstable. Energies expressed as per cent of the laminar Couette flow energy.

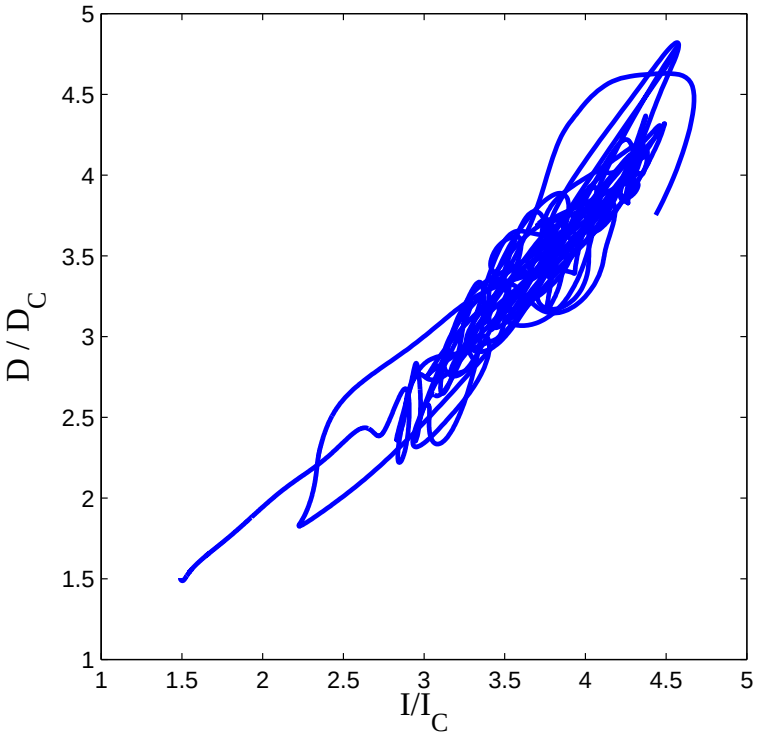

FIGURE 22. Projection of the trajectory of the SSST dynamics during transition from the laminar roll/streak state (lower left point in trajectory) to the time dependent state on the input rate, I, and dissipation rate, D, plane, both normalized by their values for the laminar Couette flow for the transition to the time dependent roll/streak state shown in Fig. 21.

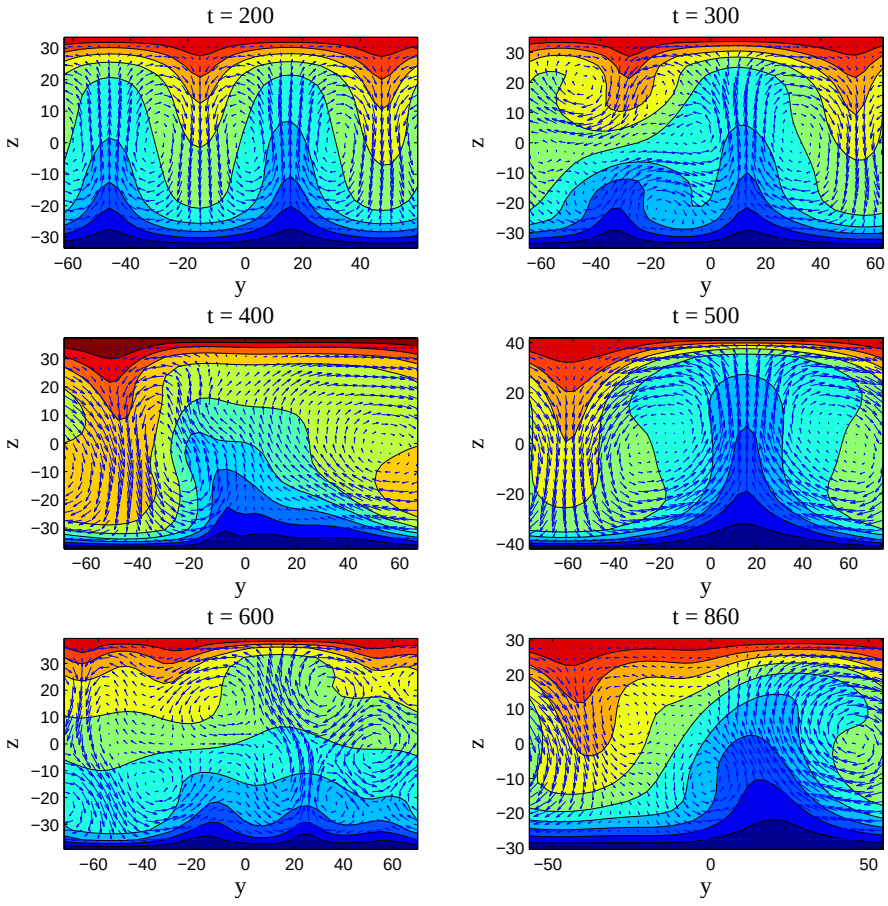

FIGURE 23. Time dependent roll-streak states at $f = 10$ corresponding to the evolution shown in Fig. 21. The equilibrium roll/streak/turbulence complex is structurally unstable at this value of f and this instability leads to emergence of a time dependent state. Shown are snapshots of the streamwise mean streamwise flow (contours) and vectors of the spanwise/cross-stream flow. The channel size is indicated in wall units. At $t = 200$ the streamwise flow has become perturbation unstable. The time dependent state is characterized by streaks with mean spacing of about 100 wall units that episodically collapse (panel for $t = 600$) and, reform. At times the flow remains for an interval close to the structurally unstable laminar roll/streak state ($t = 860$).

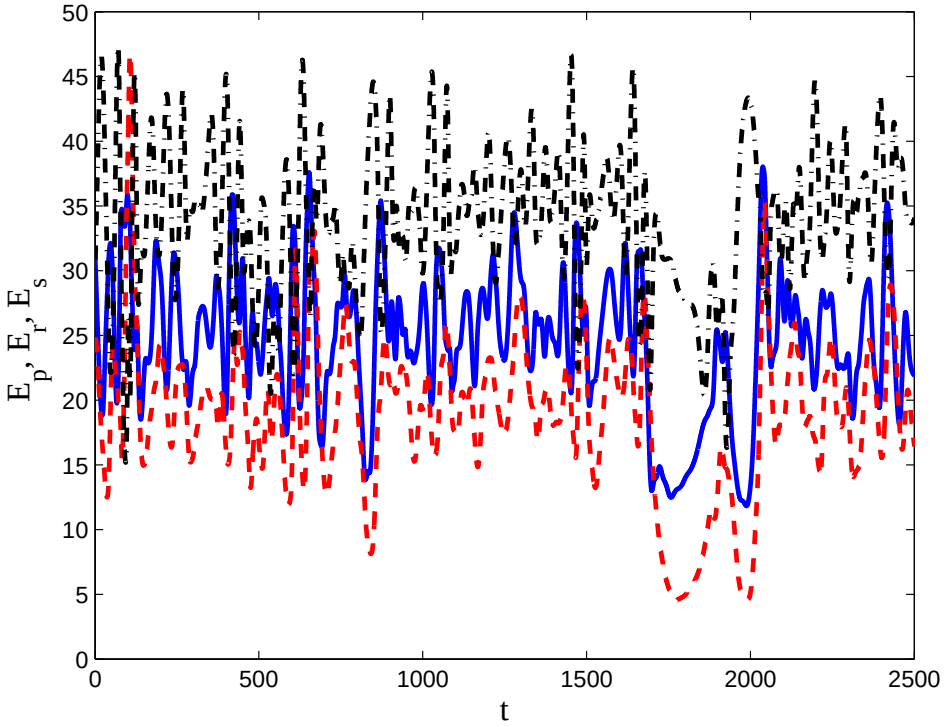

FIGURE 24. Eddy kinetic energy $100\sqrt{E_p/E_C}$ (solid), roll energy $100\sqrt{E_r/E_C}$ (dashed) and streak energy $100\sqrt{E_s/E_C}$ (dash-dot) for $f = 10$. An interval of slow variation about the structurally unstable laminar roll/streak state occurs around $t = 1700$. Energies expressed as per cent of the laminar Couette flow energy. Parameters are as in Fig. 3.

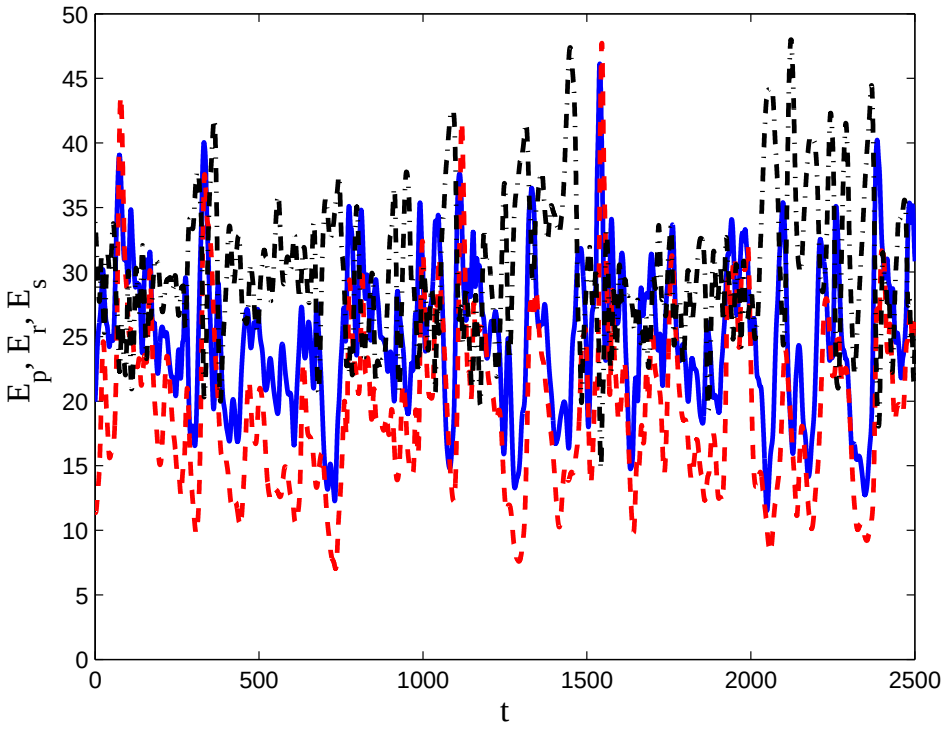

FIGURE 25. Eddy kinetic energy $100\sqrt{E_p/E_C}$ (solid), roll energy $100\sqrt{E_r/E_C}$ (dashed), and streak energy $100\sqrt{E_s/E_C}$ (dash-dot) for the self-sustained state $f = 0$. Other parameters as in Fig. 24.

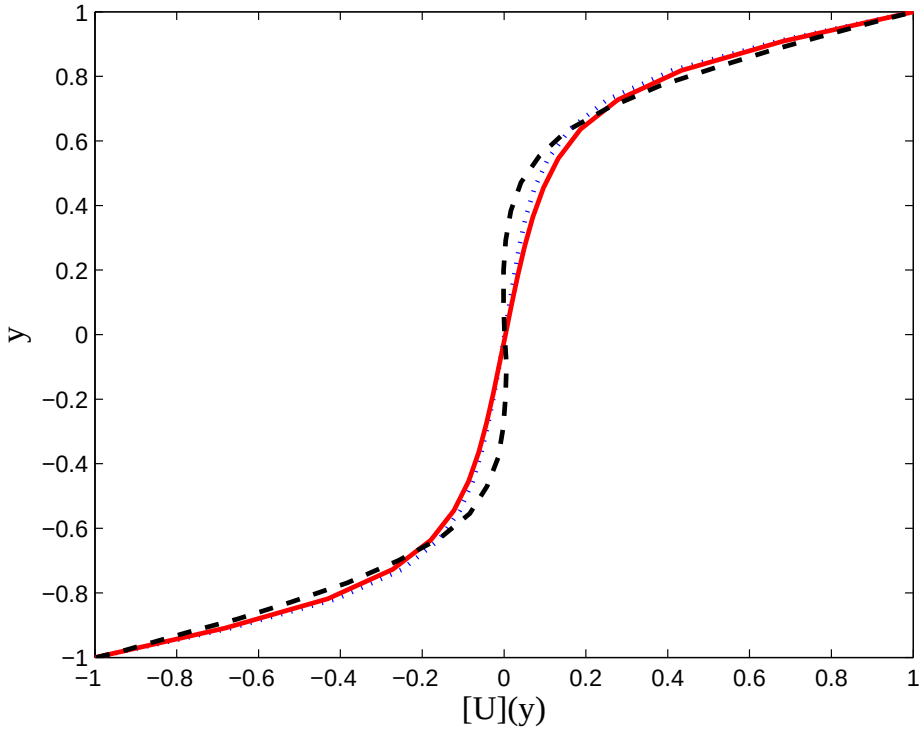

FIGURE 26. Spanwise and time averaged streamwise flow, $[U](y)$, in the self sustained turbulent roll/streak state for $f = 0$ (solid) shown in Fig. 25 and for $f = 10$ (dash-dot) shown in Fig. 24. Also shown for comparison is the time and spanwise mean under turbulent conditions from the simulation of Kawahara & Kida (2001) (dashed). The average Reynolds number based on friction velocity $R_\tau = 37$.

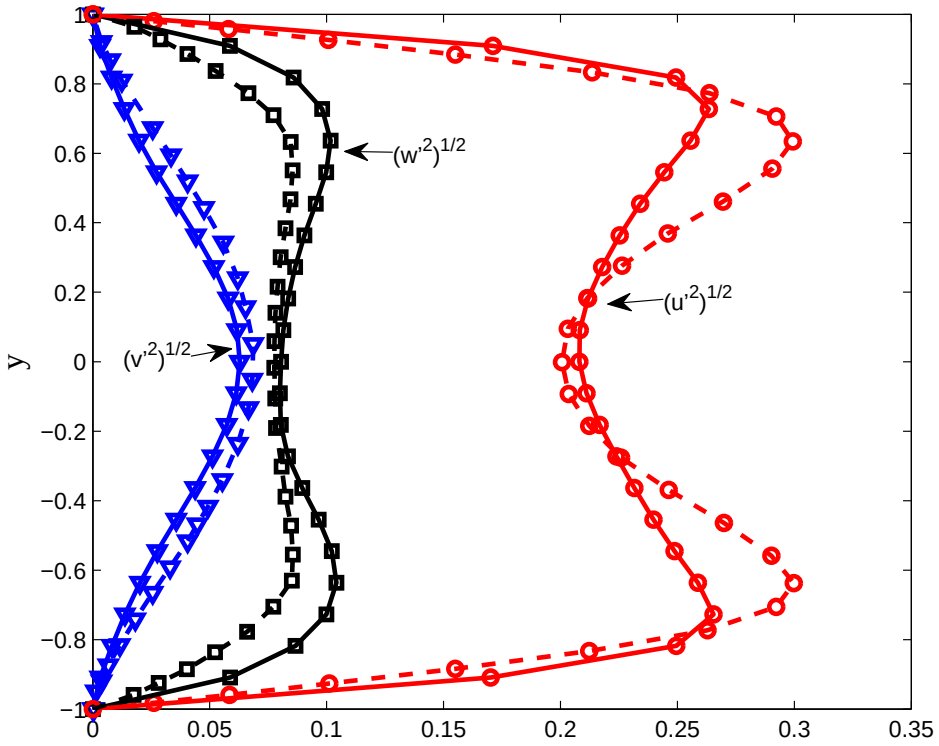

FIGURE 27. The cross-stream structure of the spanwise and time averaged RMS: streamwise velocity $\sqrt{< u^2 >}$ (solid-circles), cross-stream velocity $\sqrt{< v^2 >}$ (solid-triangles) and spanwise velocity $\sqrt{< w^2 >}$ (solid-squares) in the turbulent roll/streak state for $f = 0$ (solid) shown in Fig. 25. Also shown the corresponding quantities under turbulent conditions from the simulation of Kawahara & Kida (2001) (dashed). The average Reynolds number based on friction velocity is $R_\tau = 37$.

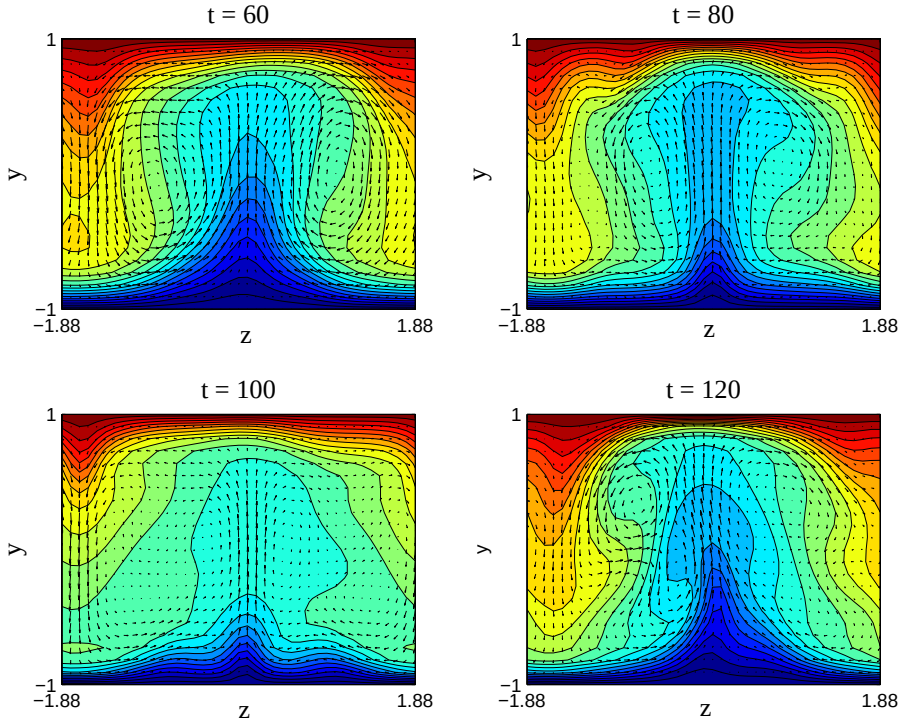

FIGURE 28. The streamwise mean roll/streak structure over an interval of streak vacillation in the self-sustained state with $f = 0$ corresponding to the evolution shown in Fig. 25.

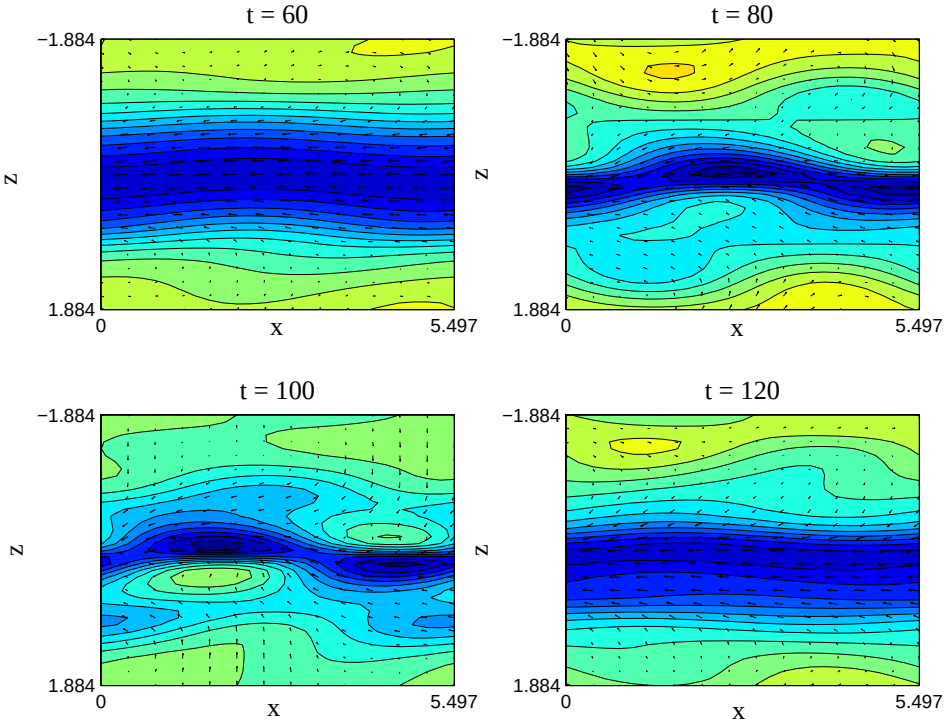

FIGURE 29. Vectors of velocity in the $(x-z)$ plane at $y=-0.75$ and contours of total streamwise velocity component in this plane at times corresponding to the roll/streak structure snapshots shown in Fig. 28.

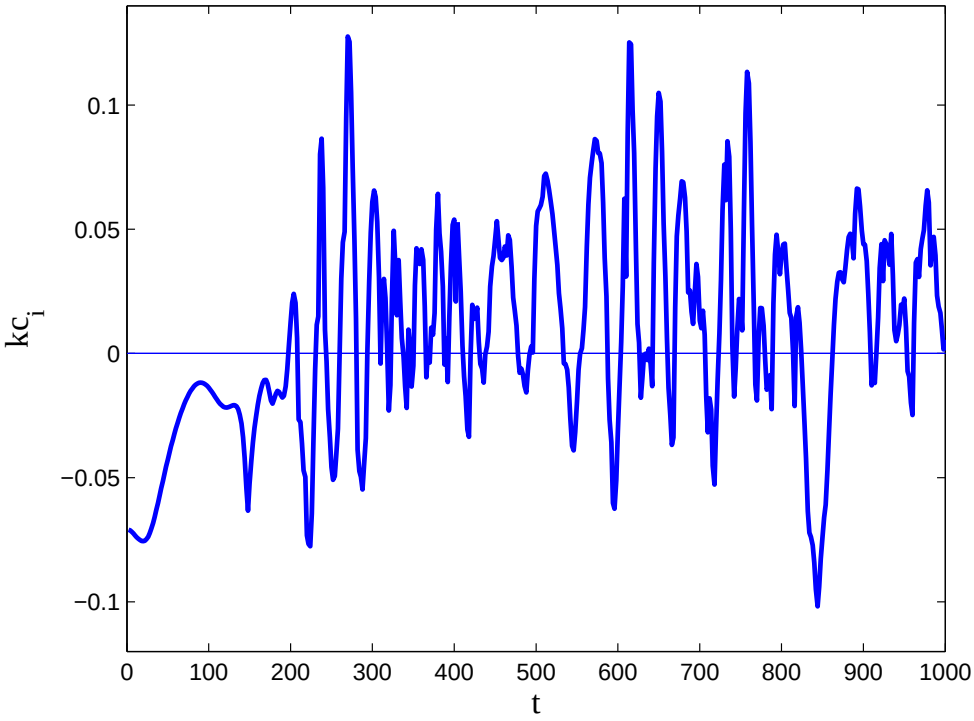

FIGURE 30. Maximum growth rate of the instantaneous streamwise flow during the transition from the roll-streak equilibrium to the turbulent state shown in Fig. 21. The essentially laminar roll-streak equilibrium is structurally unstable but perturbation stable. The streamwise mean flow becomes perturbation unstable at $t = 200$.

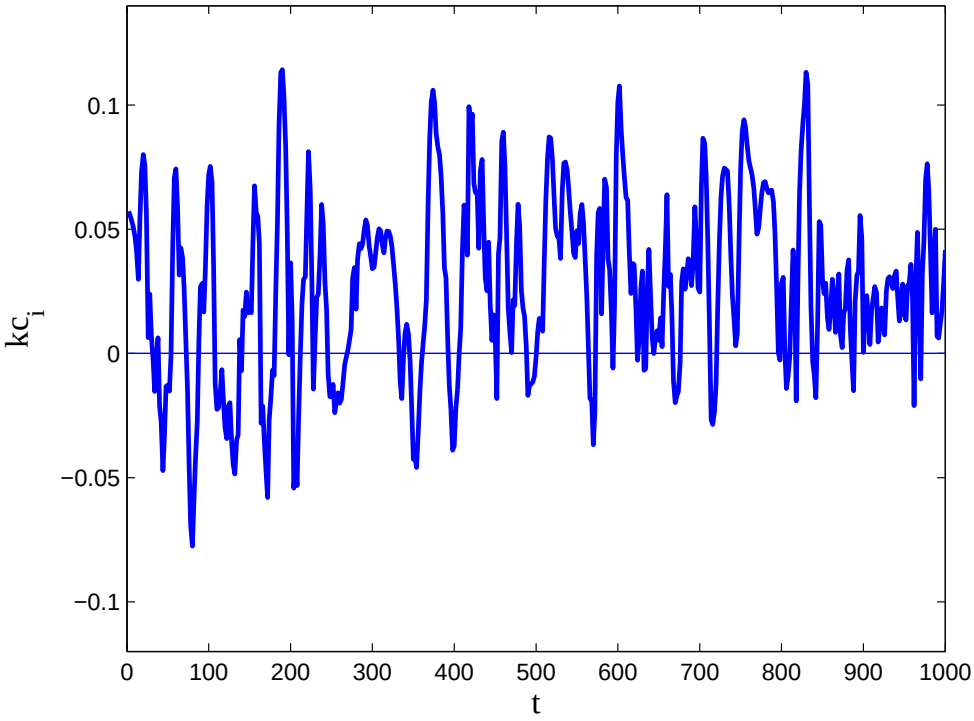

FIGURE 31. Maximum growth rate of the instantaneous streamwise flow corresponding to the time-dependent roll/streak/perturbation state for $f = 0$ shown in Fig. 25.

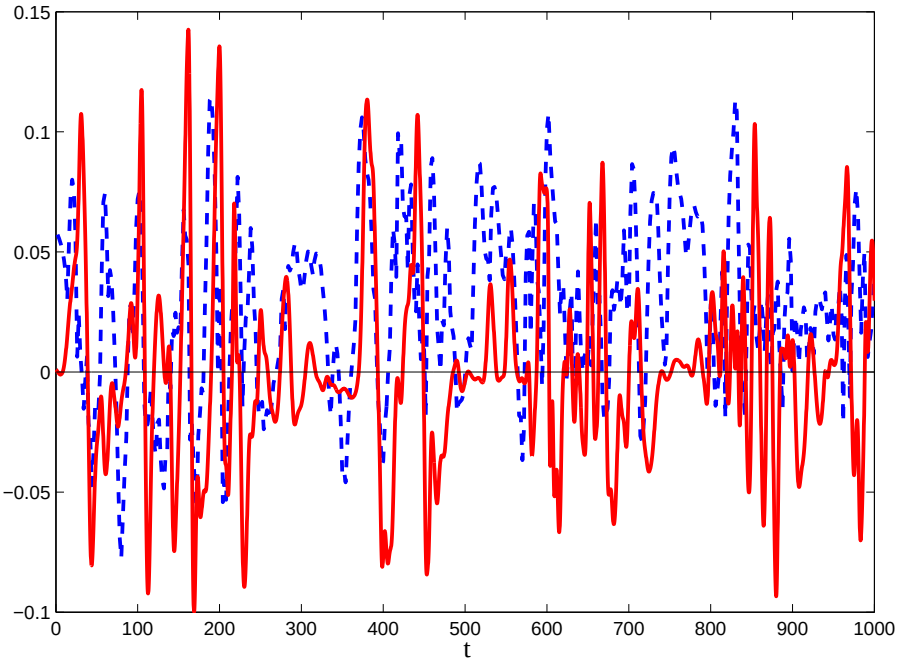

FIGURE 32. Instantaneous eddy growth rate $d(\log\sqrt{E_p})/dt$ (solid), and maximum modal growth rate of the instantaneous flow (dashed) for the time-dependent roll/streak/perturbation simulation shown in Fig. 25. The correlation coefficient of these growth rates over the whole simulation is 0.2.

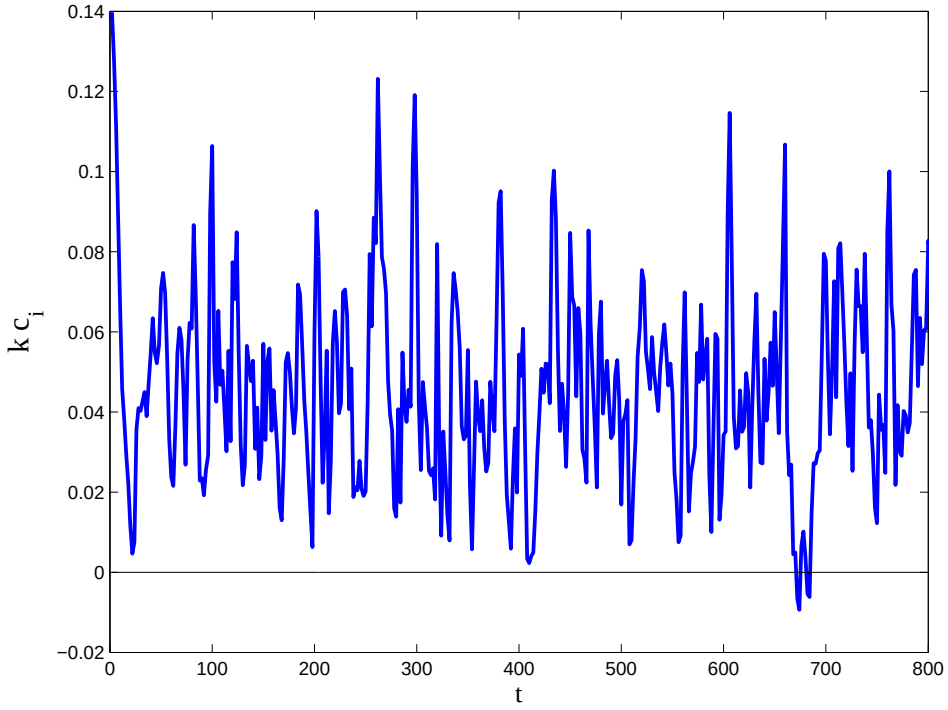

FIGURE 33. Maximum growth rate of the instantaneous streamwise flows corresponding to the time-dependent roll/streak/perturbation state for $R = 800$. Note that this time dependent state at $R = 800$ is more unstable than the time dependent state at $R = 400$. There is no forcing, $f = 0$.

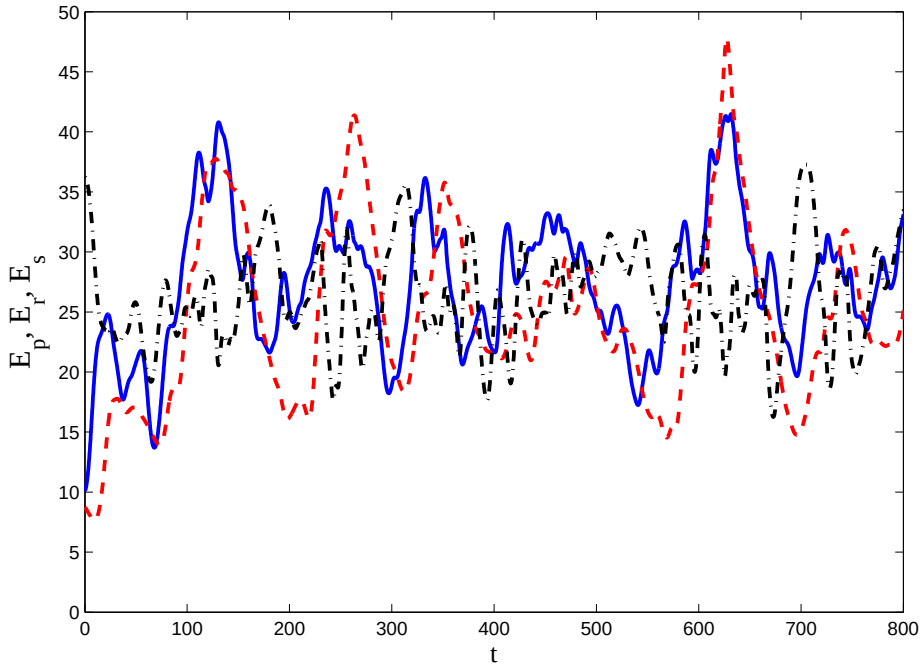

FIGURE 34. Eddy kinetic energy $100\sqrt{E_p/E_C}$ (solid), roll energy $100\sqrt{E_r/E_C}$ (dashed), and streak energy $100\sqrt{E_s/E_C}$ (dash-dot) for the time-dependent state for $R = 800$ and $f = 0$. The corresponding instantaneous growth rates are shown in Fig. 33.

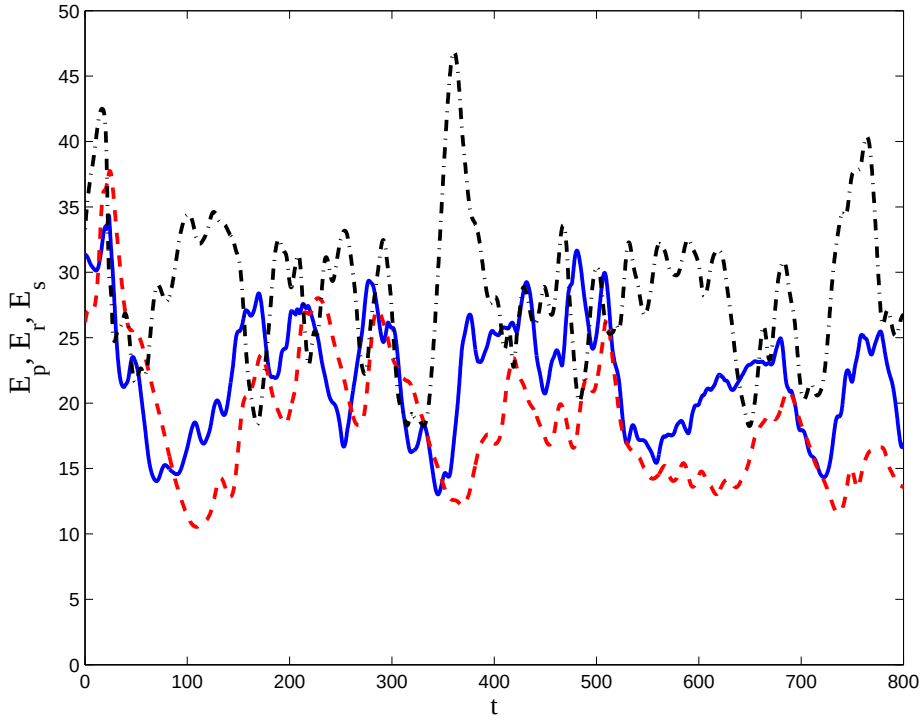

FIGURE 35. Eddy kinetic energy, $100\sqrt{E_p/E_C}$ (solid), roll energy $100\sqrt{E_r/E_C}$ (dashed) and streak energy $100\sqrt{E_s/E_C}$ (dash-dot) in the self-sustained time-dependent state for $f = 0$ at $R = 800$. The flow has been made perturbation stable at each instant in the following manner: all unstable eigenfunctions have been ascribed growth rate -0.001 while their phase speed has not been changed. It was verified that the maximum growth rate of the flow at each instant is at most -0.001. Despite being perturbation stable at each instant the time dependent state is sustained by the parametric non-normal growth process. This modification of the growth resulted in a time dependent state with stronger streaks. Other parameters are as in Fig. 33.

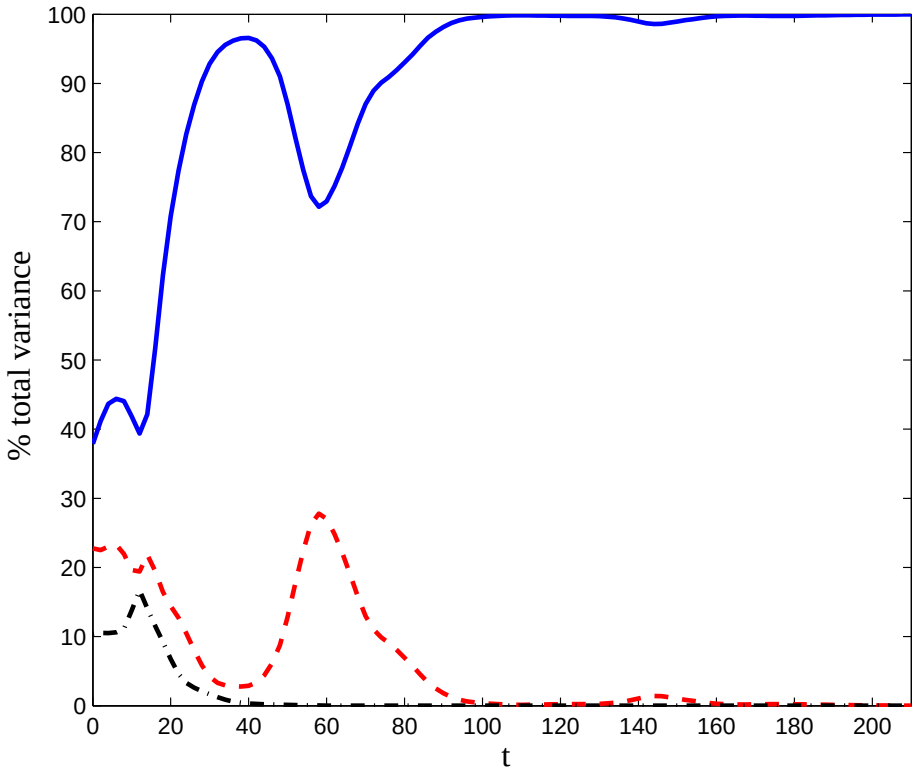

FIGURE 36. Percentage eddy energy accounted for by the first three EOF's of the eddy covariance matrix with $f = 0$ (first EOF: solid, second EOF: dashed, third EOF: dash-dot). The eddy covariance at $t = 0$ is that maintained by excitation parameter $f = 10$ and is full rank. When the excitation is removed the covariance is rapidly collapses to rank 1, and the eddy structure becomes the Lyapunov vector associated with zero Lyapunov exponent of the time dependent equation (11.1). Parameters correspond to channel: length $L_x = 1.75\pi$, spanwise width $L_z = 1.2\pi$, half cross-stream height $L_y = 1.0$ and the Reynolds number is $R = 400$. The perturbation streamwise wavenumber, $k = 1.143$, corresponds to the gravest mode in the channel. Parameters are as in Fig. 3.

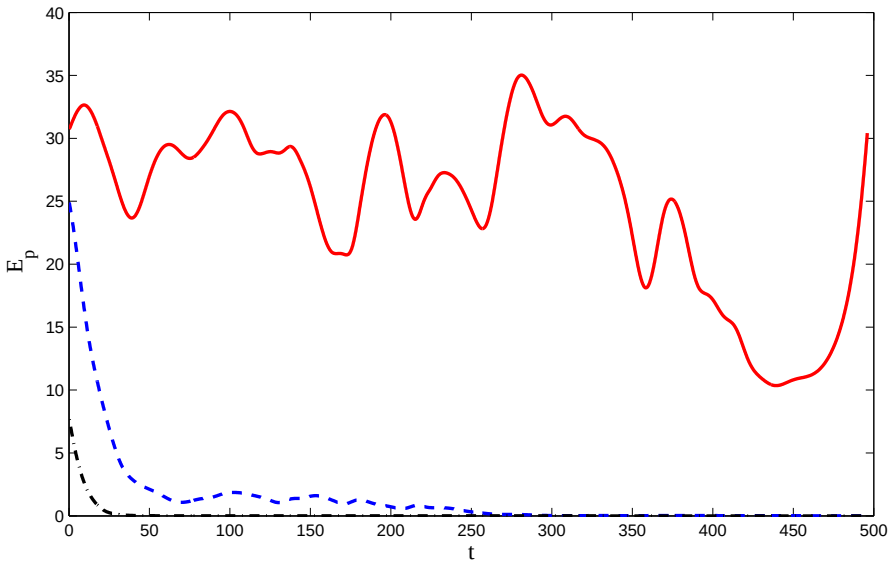

FIGURE 37. Eddy kinetic energy $100\sqrt{E_p/E_C}$ for the component with streamwise wavenumber $k_0 = 1.143$ (solid), for wavenumber $k_0/2$ (dashed), and for wavenumber $2k_0$ (dash-dot). The eddy covariance at $t = 0$ is that maintained under excitation of each eddy component with $f = 10$. When the excitation is removed the mean eddy energy becomes rapidly concentrated in a single wavenumber with associated rank 1 covariance. Parameters as in Fig. 36.

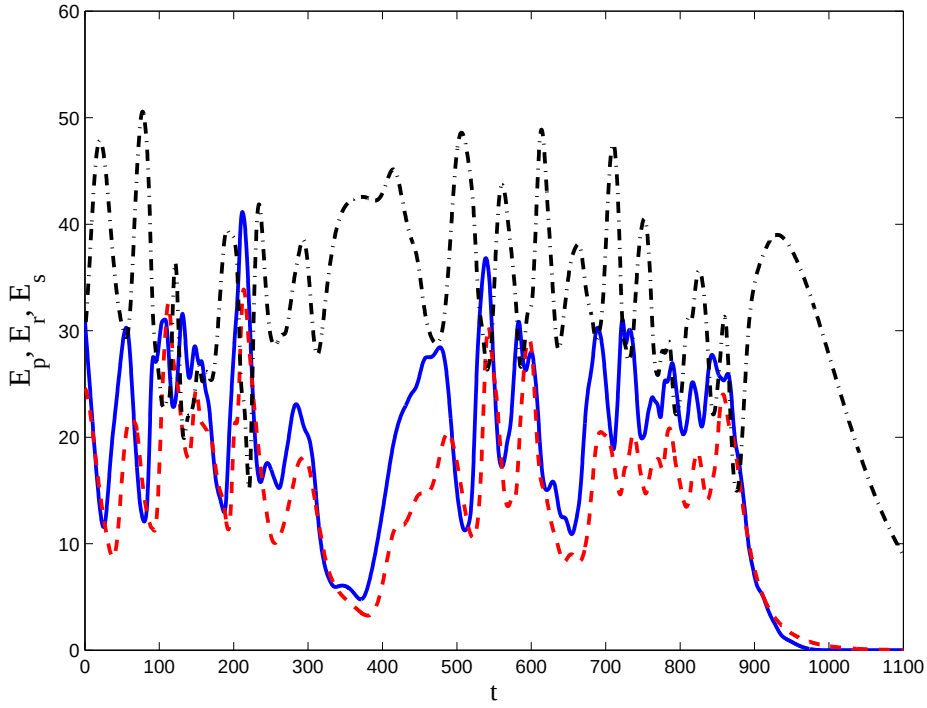

FIGURE 38. Eddy kinetic energy $100\sqrt{E_p/E_C}$ (solid), roll energy $100\sqrt{E_r/E_C}$ (dashed) and streak energy $100\sqrt{E_s/E_C}$ (dash-dot) in the time-dependent state with $f = 0$ and $R = 350$. The perturbation streamwise wavenumber, $k = 1.143$, corresponds to the gravest mode in the channel.